A Statistical Study of Frictional Wind Veering in the Planetary Boundary Layer

by
Bruce R. Mendenhall

Technical Paper No. 116
Department of Atmospheric Science
Colorado State University
Fort Collins, Colorado

Colorado State University

Department of Atmospheric Science

Paper No. 116

A STATISTICAL STUDY OF FRICTIONAL WIND VEERING IN THE PLANETARY BOUNDARY LAYER

by

Bruce R. Mendenhall

This report was prepared with support from

NSF GF-177
ESSA E-34-67(G)

Department of Atmospheric Science
Colorado State University
Fort Collins, Colorado

December 1967

Atmospheric Science Paper No. 116

TABLE OF CONTENTS

ABSTRACT

Despite the general applicability of classical Ekman theory, individual observations of wind veering in the planetary boundary layer seldom exhibit the typical spiral turning with height. This study attempts to assess the reasons for these deviations from theory which occur not only as large fluctuations in time but also as significant differences in mean profiles from one location to another.

The magnitude of the short-term eddy fluctuations is large in comparison to average frictional veering. A statistical analysis of sufficiently long periods of observational data is made in order to eliminate these small-scale variations. An assessment of the large-scale veering parameters is then possible.

Wind tower and conventional rawinsonde veering data of three to five year periods from various land and ocean stations are objectively analyzed. Average wind profiles and statistics of the individual observations in the lowest two kilometers are computed in order to determine which parameters significantly affect frictional wind veering. Corrections to observed veering are made for the horizontal temperature gradient (rotation of the pressure gradient with height) and for variations of thermal stability. The relative importance of these corrections and the nature of their variability in different climatic regions are discussed.

After statistically eliminating the unsteady effects and applying corrections for horizontal and vertical temperature gradients, a more realistic spiral is obtained at each station.

INTRODUCTION

It has generally been assumed that the wind in the planetary boundary layer of the Northern Hemisphere always veers[1] with height due to frictional drag at the earth's surface. However, observational evidence corroborates this assumption only in a very general sense. For example, Fig. 1 shows a time-series of wind veering in the lowest km at Swan Island, West Indies. The large variability portrayed by this diagram is typical of wind veering in the relatively steady trade-wind zone. An example from Weather Ship N in the sub-tropical Pacific is shown in Fig. 2. In addition to great variability of veering, nearly half of the soundings indicate backing of the wind with height. Typical observations such as these lead one to speculate on the physical processes taking place in the planetary boundary layer.

One of the early observations that aroused curiosity about this subject came from the famous drift of the Fram, late in the nineteenth century. An important finding from this expedition was that the Arctic ice-pack drifted 20° to 40° to the right of the surface wind. Nansen (1902) attributed this to the effect of the earth's rotation and inspired Ekman (1902) to confim his hypothesis mathematically. Ekman, in his well-known work of 1905, put forth the theory of a wind-driven current in an infinite ocean and derived the spiral profile that carries his name. Åkerblom (1908) theoretically extended the Ekman spiral to the atmosphere, and from Eiffel Tower measurements, he showed

---

[1] The term "veering" indicates clockwise rotation. Hereafter, "veering", used alone, will imply clockwise rotation of the wind with height in the lowest km. "Backing" is equivalent to negative veering.

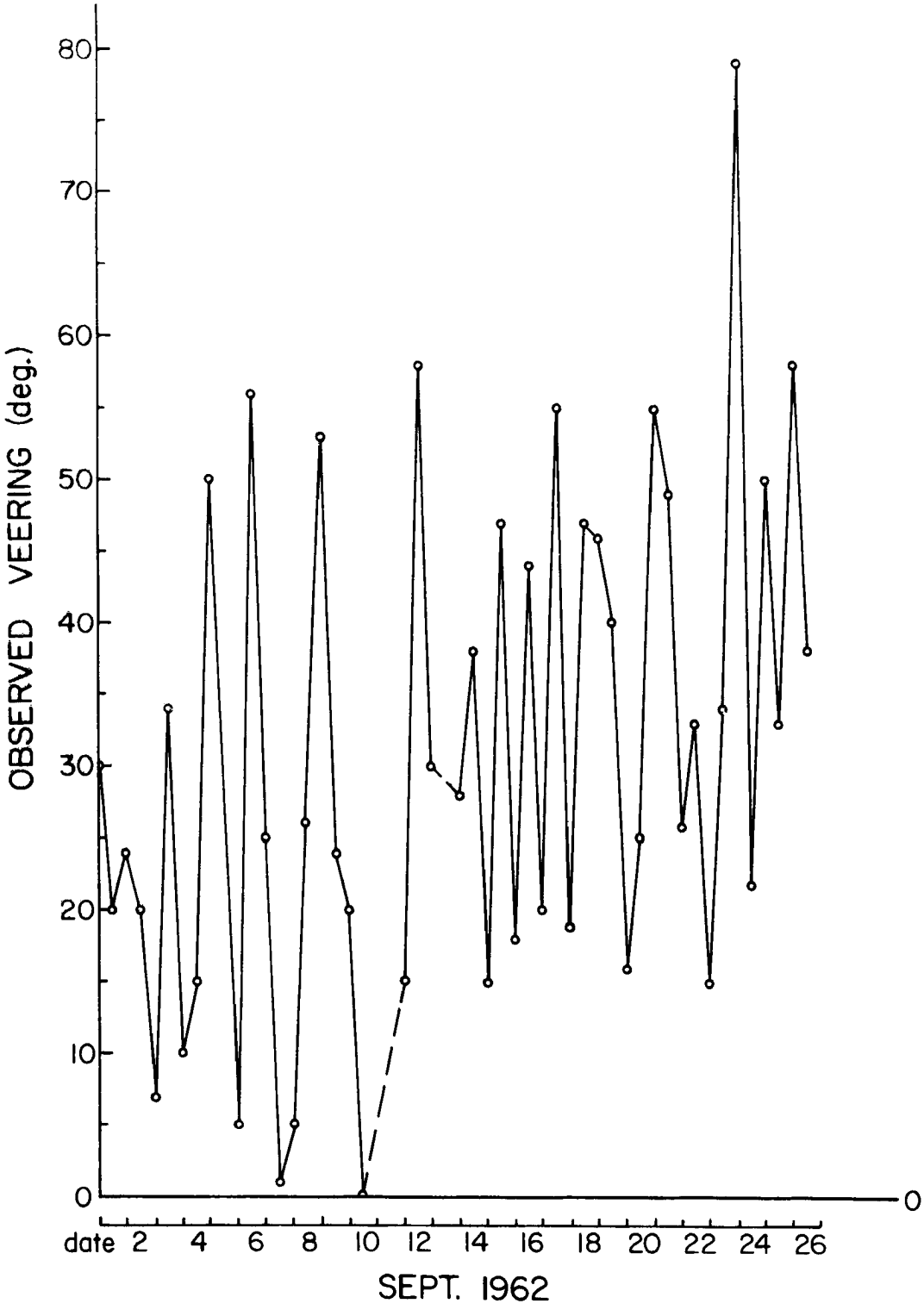

Fig. 1. Time-series of observed wind veering in lowest km layer at Swan Island obtained from 12-hourly rawin soundings. Note the typical variability of veering. Dashed lines indicate periods of missing observations.

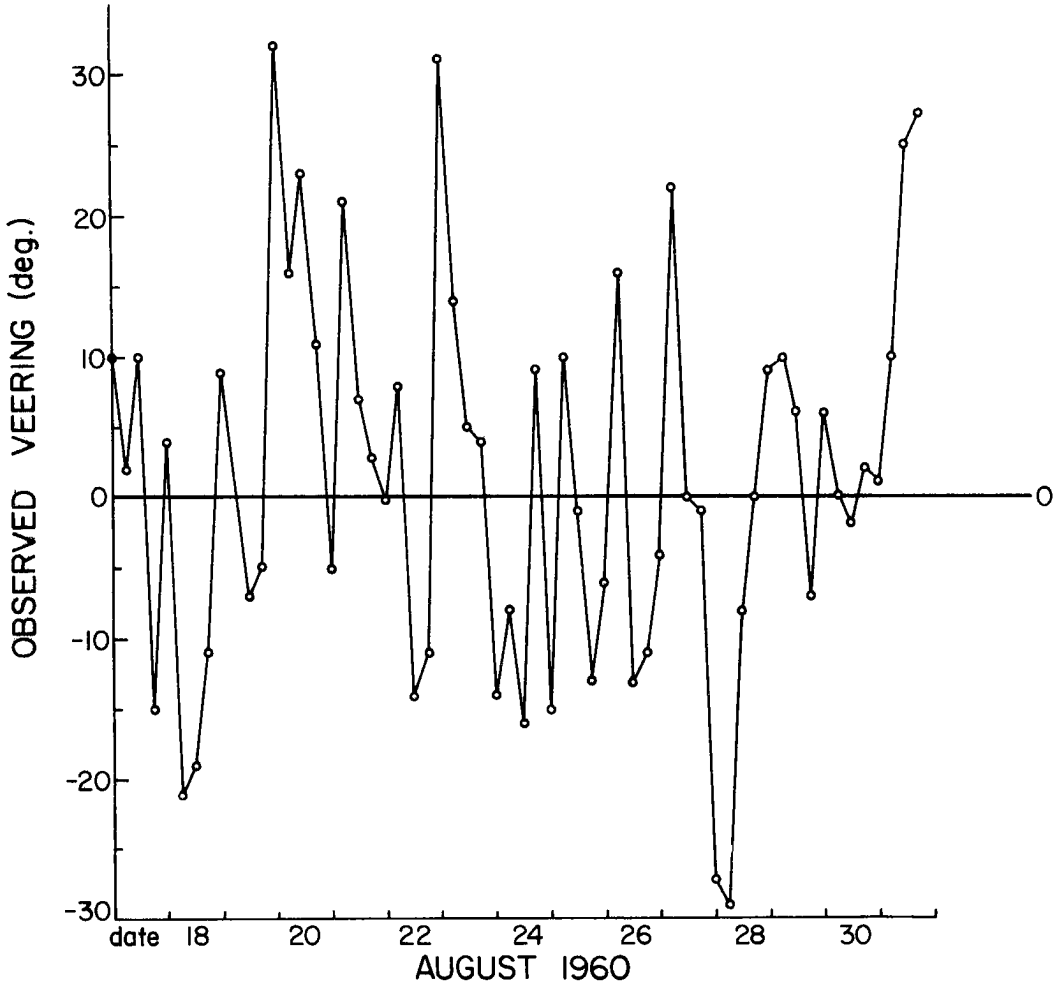

Fig. 2. Time-series of observed wind veering in lowest km layer at Ship N obtained from 6-hourly rawin soundings. Note the considerably smaller average veering than at Swan Island. A large percentage of the observations indicate backing of the wind with height.

that there is a general observational comparison with theory. Taylor (1916) refined the theory to include a surface layer of constant stress and wind direction and a higher layer of decreasing stress and wind veering.

Since the early work of Ekman, Åkerblom, and Taylor, many other investigators have attempted to improve our knowledge of the veering process. Most of these efforts have been theoretical. Notable for their exhaustive treatments have been the developments of Rossby and Montgomery (1935) and of Frost (1948). These and other refined treatments have failed, however, to explain the variable character of wind veering in both the individual observations and the long-term averages at different locations. The problem is a difficult one which requires both theoretical and observational considerations. In order to obtain mathematical answers, the theoretical treatments have been overly simplified. These simplifications have, in general, been of little help in explaining either the spatial or temporal variations of frictional veering.

This study is an observational approach to the problem. Boundary layer veering is studied from a statistical point of view. The goal is to eliminate the random observational and turbulent variations of veering by considering large data samples. Average values of veering can then be compared with large-scale parameters at various locations to determine the influence of these parameters on the frictional veering.

The few previous observational studies of frictional veering have been limited in time and space.[2] In order to remove the time limita-

---

[2]Special studies using double and triple theodolite observations have been carried out over periods of one day to one month. The high accuracy of the measurements has made possible interesting calculations of Reynold's stresses, exchange coefficients, and other turbulence parameters. Some examples and the locations of their measurements are Mildner (1933): Leipzig, Germany; Sheppard et al. (1952): Scilly (island), England; Charnock et al. (1956): Anegada, Virgin Is.; Lettau and Hoeber (1964): Helgoland (island), Germany.

tion, rawinsonde data are used in the present study instead of the more accurate but less abundant special observations. A sacrifice of instrumental accuracy for a large data sample is justified by the fact that instrumental errors are considerably smaller than the turbulent variability of veering (cf. appendix). Thus, a large data sample is more likely to be of value than highly accurate data.

The use of rawinsonde data also solves the problem of spatial representation--these observations are routinely available from widely separated locations having many different environmental characteristics.

Data Sources

Table 1 summarizes the station locations and periods of record of the stations which make up the data sample. Two temperature and four wind observations per day were generally available.

TABLE 1

Summary of station locations and periods of record.

station name	location		period of record
Shreveport, La.	33°N	94°W	1963-1965
Jackson, Miss.	33	90	"
Fort Worth, Tex.	33	97	"
Little Rock, Ark.	35	92	"
Lake Charles, La.	30	93	"
Johnston Island	17	170	1960-1964
Swan Island	17	84	1959-1964
Weather Ship N	30	140	1960-1964
" I	59	19	1951-1960
" J	53	20	1951-1958
WKY-TV Tower, Okla.	36	97	March 1967

The locations of these stations are shown on the map of Fig. 3.

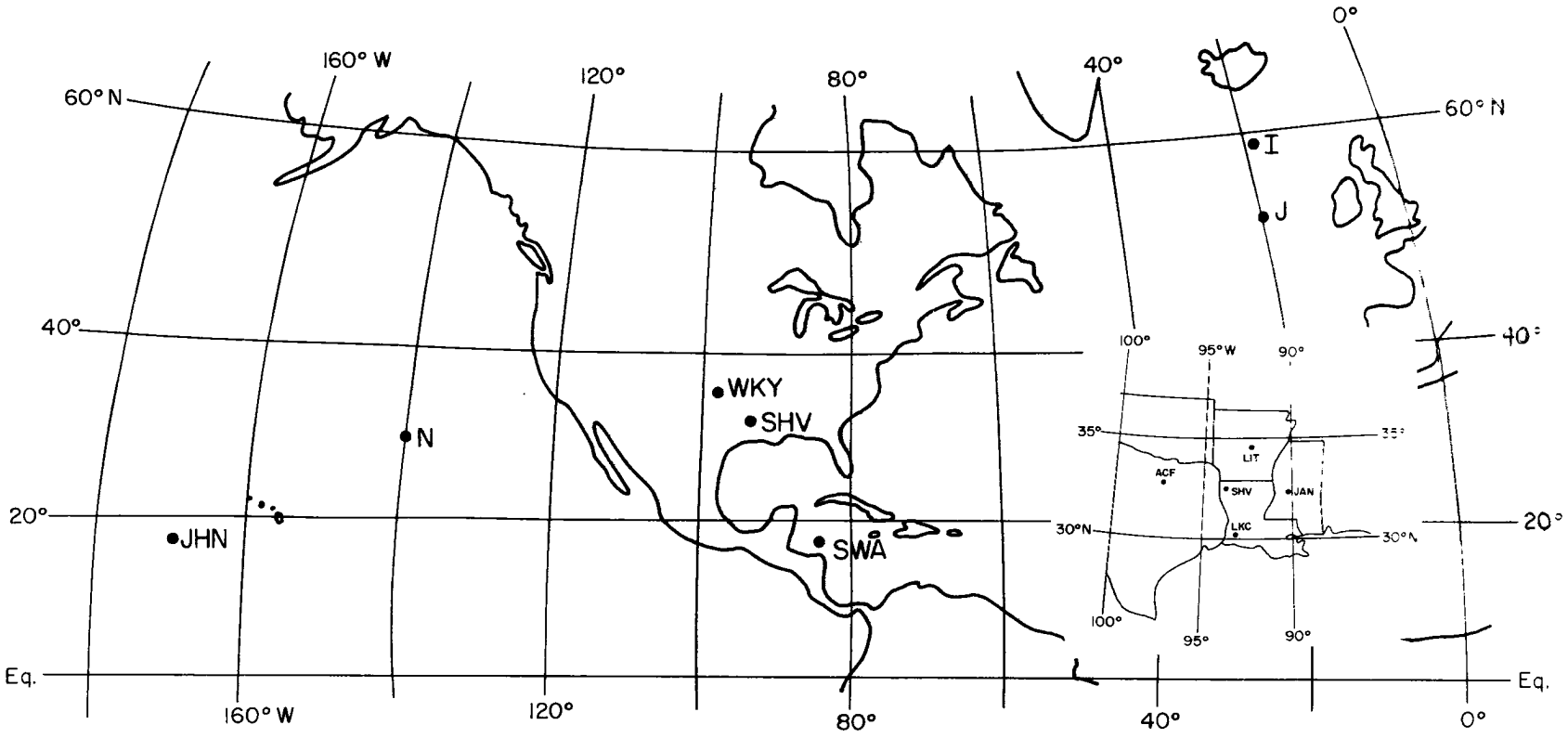

Fig. 3. Map showing locations of stations in data sample. Legend: JHN--Johnston Island; WKY--Oklahoma City tower; SHV--Shreveport; SWA--Swan Island. Single letters designate Weather Ships. The inset shows the radiosonde stations surrounding Shreveport; LIT--Little Rock; JAN--Jackson; LKC--Lake Charles; ACF--Fort Worth.

Shreveport was selected to represent mid-latitude continental conditions. This station has fairly smooth terrain in its vicinity and is surrounded by four nearly equally spaced radiosonde stations (listed in Table 1) in a pattern suited to determination of zonal and meridional temperature gradients. Data for these stations consisted of magnetic tape images of card deck 645, stored at the National Weather Records Center, Asheville, N. C. This deck includes pertinent meteorological data at 50 mb pressure increments through the levels of interest.

Johnston Island was chosen to represent an eastern ocean trade-wind regime and Ship N, the sub-tropical oceans. Constant height wind data from the surface through 2 km (card deck 535) were also available to give more detailed information at these stations. Swan Island, a western oceanic trade-wind regime, was used for comparison with Johnston Island.

Data from Weather Ships I and J, summarized by Findlater et al. (1966) were selected as typical of mid- and high-latitude ocean areas. Only limited comparison is made with the other stations.

Microfilmed records of the original wind and temperature traces from the WKY-TV tower, Oklahoma City, were obtained from the National Severe Storms Laboratory to gain insight into the small-scale time and lapse rate variations of veering.

Procedure

In addition to the gust-scale variations, several other complications arise in the planetary boundary layer such that the simple spiral wind profile is seldom observed. It is necessary to remove the assumptions upon which a spiral solution is based that are at variance

with the real atmosphere. The major causes of observational deviation from Ekman theory are:

1. Measurement errors
   a. extraneous balloon motion
   b. incorrect tracking
2. Curvature effects
3. Gust-scale accelerations
4. Large-scale horizontal temperature gradient variations
5. Large-scale vertical temperature gradient variations

Assuming that the first three deviations are essentially of a random nature, they can be eliminated in the statistical treatment by taking long-term averages. This study then concentrates on describing the latter two large-scale temperature gradient influences. Ekman theory assumes no veering of the geostrophic wind or pressure gradient with height and no variation of the vertical exchange coefficient with height. The latter two influences are directly related to the observed veering variations and can be measured. In this paper these variations of horizontal and vertical temperature gradients will be quantitatively studied. A qualitative discussion of the first three influences is given in the appendix.

THE INFLUENCE OF A HORIZONTAL TEMPERATURE GRADIENT ON OBSERVED VEERING

In the planetary boundary layer the pressure gradient force balances the sum of the Coriolis and frictional forces, assuming no curvature or other accelerations. A change with height of the pressure gradient therefore will change the vertical wind profile. In particular, if the pressure gradient rotates with height then the wind veering will be affected.

The horizontal temperature gradient is related to the pressure gradient through the thermal wind equations:

$$\frac{\partial u_g}{\partial z} = -\frac{g}{f\,\overline{T}_v}\left(\frac{\partial T_v}{\partial y}\right)_p \quad ; \quad \frac{\partial v_g}{\partial z} = \frac{g}{f\,\overline{T}_v}\left(\frac{\partial T_v}{\partial x}\right)_p \qquad (1)$$

and the geostrophic wind equations:

$$\frac{\partial p}{\partial x} = \rho f v_g \quad ; \quad \frac{\partial p}{\partial y} = -\rho f u_g \qquad (2)$$

where

p = pressure

ρ = density

f = Coriolis parameter

g = acceleration of gravity

T_v = virtual temperature

z = height

u_g = geostrophic wind component in x-direction

v_g = geostrophic wind component in y-direction

In eqs. (1) the temperature gradient is of virtual temperature on a constant pressure surface. This is very close, numerically, to the horizontal temperature gradient and will be assumed the same in this paper.

In order to show the importance of pressure gradient rotation, the typical Ekman theory will now be expanded to include a horizontal temperature gradient. Assuming horizontal steady motion, negligible horizontal wind shear, and eddy viscosity and density constant with height, the equation of motion may be written, following Hess (1959), as

$$\frac{\partial p}{\partial x} + i\frac{\partial p}{\partial y} + \rho f i(u+iv) - \rho K\frac{\partial^2}{\partial z^2}(u+iv) = 0 \qquad (3)$$

where $i = (-1)^{\frac{1}{2}}$ and K is the eddy viscosity coefficient. With the assumption of constant horizontal temperature gradient with height, $\frac{\partial^2 u_g}{\partial z^2} = \frac{\partial^2 v_g}{\partial z^2} = 0$ through eqs. (1). Thus substituting eqs. (2) into the first two terms of eq. (3) yields the easily solved differential equation:

$$\frac{\partial^2}{\partial z^2}(u+iv-u_g-iv_g) - \frac{if}{K}(u+iv-u_g-iv_g) = 0.$$

With boundary conditions of vanishing flow at the surface and geostrophic flow at an upper, infinitely high level, the solution is:

$$u+iv-u_g-iv_g+(u_g+iv_g)e^{-(1+i)az} = 0.$$

Separating real and imaginary parts, the final equations become:

$$\begin{aligned} u &= u_g(1-e^{-az}\cos az) - v_g(e^{-az}\sin az) \\ v &= u_g(e^{-az}\sin az) + v_g(1-e^{-az}\cos az) \end{aligned} \qquad (4)$$

where $u_g = u_{g0} - \frac{g}{fT} \cdot \frac{\partial T}{\partial y} z$ and $v_g = v_{g0} + \frac{g}{fT} \cdot \frac{\partial T}{\partial x} z$ from eqs. (1), u_{g0} and v_{g0} are the surface geostrophic wind components, and $a = (f/2K)^{\frac{1}{2}}$.

In the above, steady flow and a constant vertical exchange coefficient have been assumed. Effects of variable thermal stratification and unsteady flow are discussed in later sections.

Figs. 4 and 5 show the distortion of the Ekman spiral due to a horizontal temperature gradient with different values of eddy viscosity, temperature gradient, and latitude, following eqs. (4). The number on each hodograph indicates the wind veering angle between 150 m and 1000 m. Using 150 m as the lower level is the same as assuming a surface layer of constant stress and wind direction of 150 m thickness. Each figure includes eight hodographs for surface geostrophic wind from each octant.

The theoretical hodographs of Figs. 4 and 5 can be compared with actual observations from similar environmental conditions. Wind data at Ship N were vectorially averaged in wind direction classes of 30°. The climatological horizontal temperature gradient at Ship N varies little throughout the year and is directed with warmest temperatures approximately toward the south. Fig. 6 portrays 12 hodograph plots similar to Figs. 4 and 5, obtained by averaging u and v components at seven levels in 30° classes of surface wind direction. The veering angle between the surface and 1000 m and the number of observations are indicated on each hodograph. The influence of thermal wind is evident: southerly surface winds, though they occur much less often than northeasterly winds, are attended by considerable veering with height. Under northwest wind conditions a backing of the wind is observed.

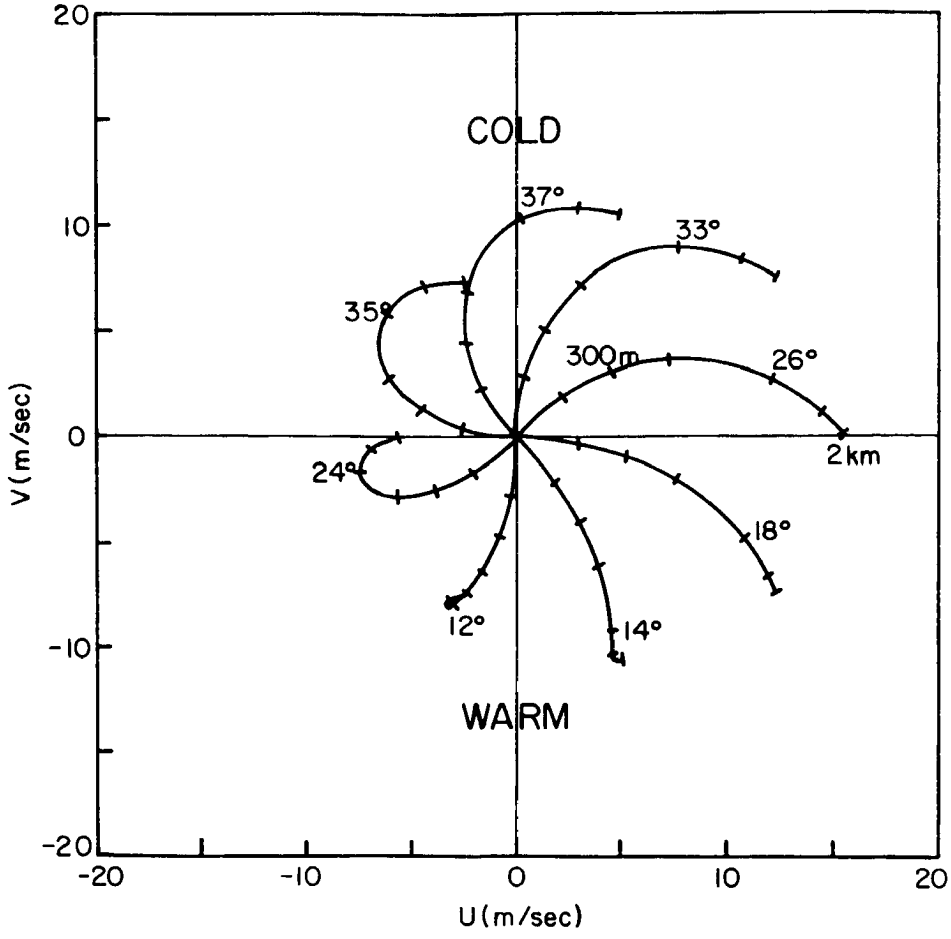

Fig. 4. Theoretical wind spirals at 30°N lat., after eqs. (4). K = 1.7 x 10^5 cm^2/sec. Temperature gradient is 5°C/1000 km with cold towards north. Numbers indicate veering in degrees between 150 and 1000 m. Elevation marks at 150, 300, 500, 1000, 1500, and 2000 m.

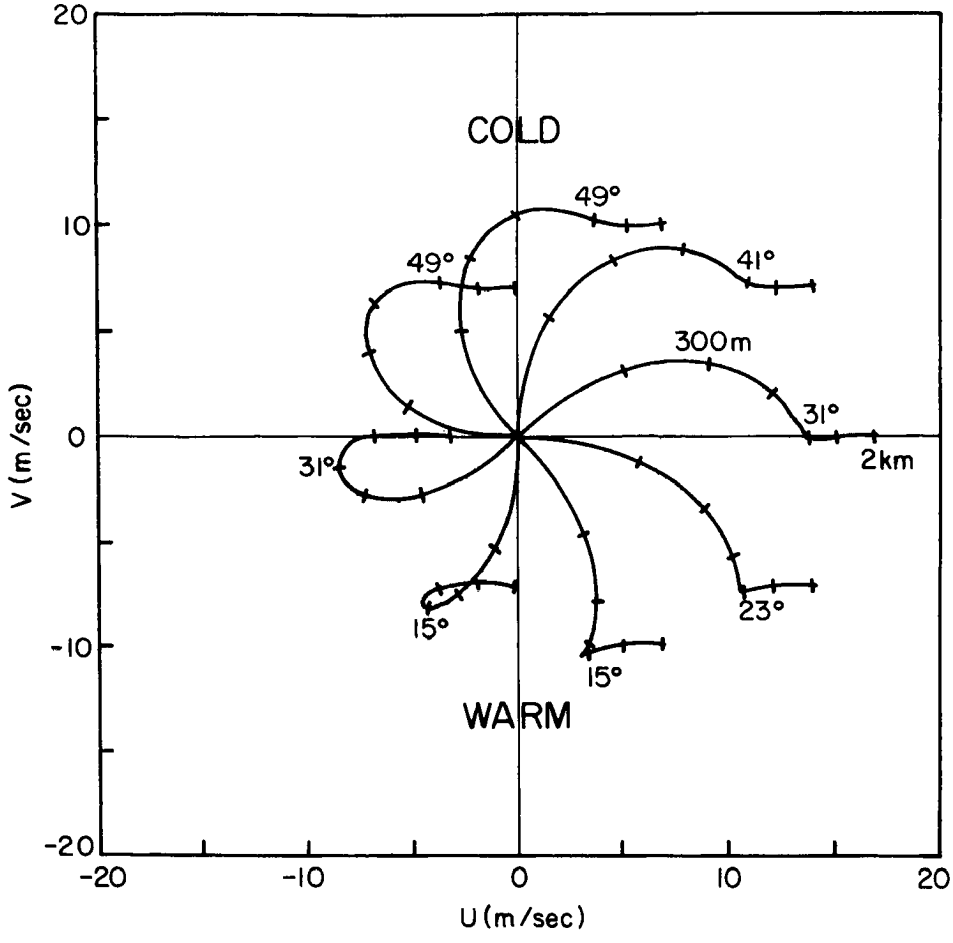

Fig. 5. Same as Fig. 4 except latitude is 43°N.
$K = 4.2 \times 10^4$ cm^2/sec, temperature gradient = 10°C/1000 km.

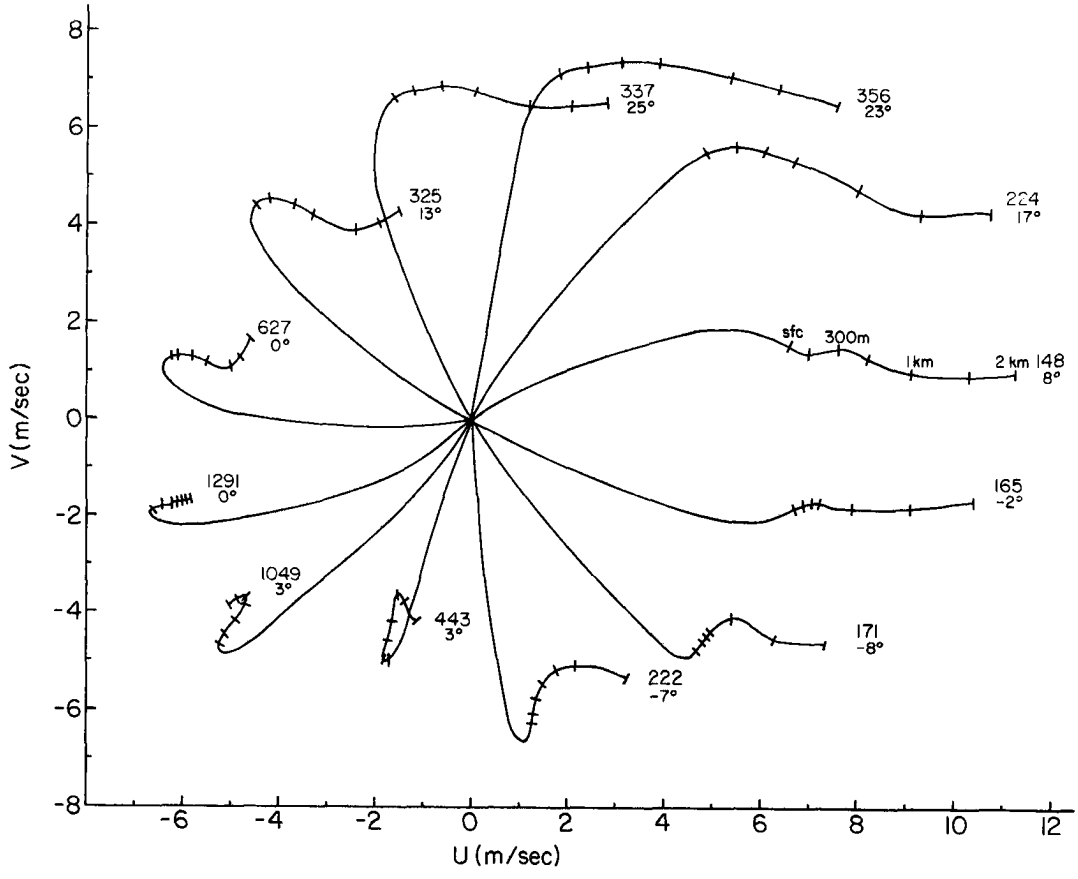

Fig. 6. Observed hodographs at Ship N for the years 1960-1964 grouped according to surface wind direction. The number of observations and the veering between the surface and 1000 m is shown on each hodograph. For example, the group with surface winds between 060° and 090° included 1291 cases with 0° average veer in the lowest km. Elevation marks are shown at the surface, 150, 300, 500, 1000, 1500, and 2000 m.

A treatment similar to that in Fig. 6 has been used by Johnson (1962) in analyzing the central U. S. kite observations of Gregg (1922), and by Lettau (1967) who utilized Antarctica pilot balloon data. Thermal wind vectors were deduced from the observed hodographs in these studies without considering the horizontal temperature gradient directly.

Significant horizontal temperature gradients are present at most stations in the individual observations and in the long-term average. Ship N and Johnston Island both have prevailing northeast surface winds. Both experience practically constant cold air advection; consequently, the geostrophic wind or pressure gradient veering with height is negative. The actual frictional veering should therefore be greater than the observed veering at these stations when correction is made for the geostrophic veering.

Fig. 7 demonstrates this geostrophic correction for the long-term average hodograph (solid curve) at Johnston Island which was obtained by vector averaging 3667 wind observations. The geostrophically corrected profile (dashed curve) is shown on the same graph. The geostrophic correction was computed from the mean annual horizontal temperature gradient near Johnston, which was obtained from monthly climatic data (Wyrtki, 1966; NAVAIR, 1966). The u and v changes of the wind with height were calculated from eqs. (1) and added to the observed wind at each level. Fig. 7 shows that the mean observed veering to the 1 km level is 4°, while the corrected, or frictional, veering is 10°. The veering difference of 6° can be interpreted as the backing with height of the geostrophic wind due to cold advection (i. e., backing of the pressure gradient with height).

Fig. 8 shows similar data for Swan Island. At this station the long-period thermal advection is nearly neutral. The observed veering

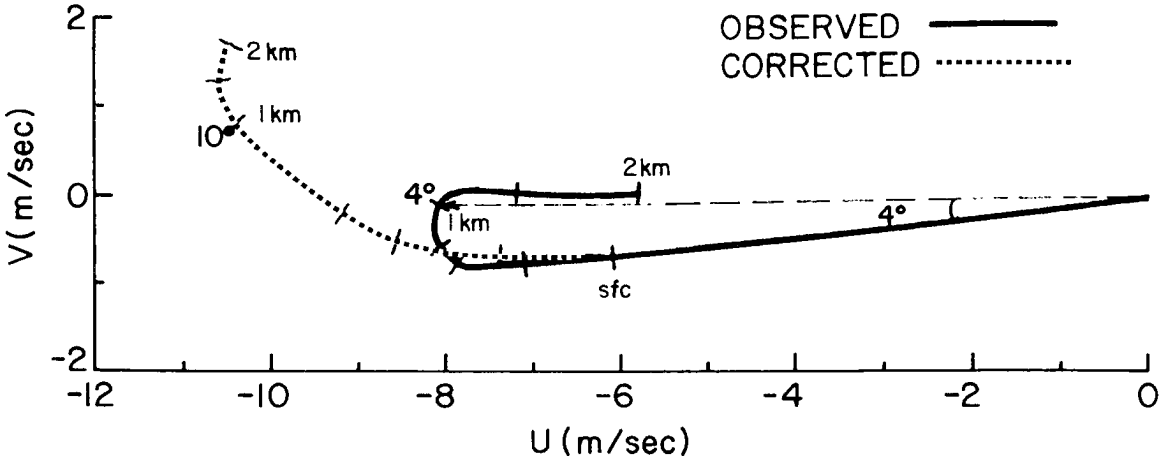

Fig. 7. Observed and geostrophically corrected hodographs at Johnston Island derived from 3667 observations. Elevation marks are shown at the surface, 150, 300, 500, 1000, 1500, and 2000 m. Veering angle between the surface and 1000 m is noted on each hodograph. Observed veering is 4° and corrected veering, 10°.

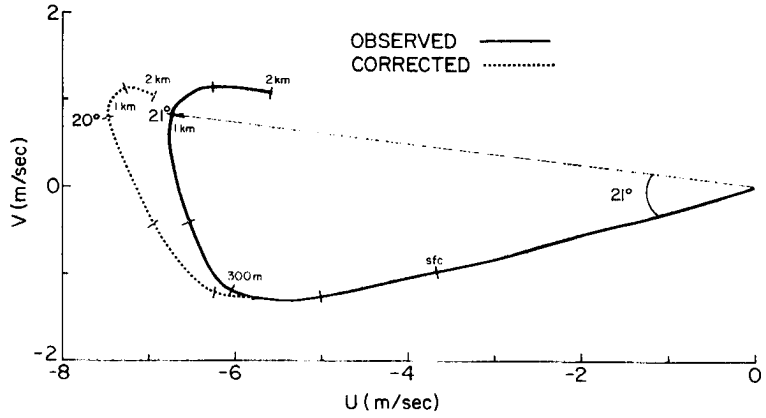

Fig. 8. Observed and geostrophically corrected hodographs at Swan Island derived from 2070 observations. Elevation marks are shown at the surface, 150, 300, 500, 1000, 1500, and 2000 m. Veering angle between the surface and 1000 m is noted on each hodograph. Observed veering is 21° and corrected veering, 20°.

is 21° and corrected veering, 20°. The larger frictional veering at Swan Island compared with Johnston Island is attributed primarily to a difference in roughness--Johnston has an area of 1 km^2 and during the period of observations, a maximum elevation of 8 m. There was virtually no land-fetch near the weather station under prevailing wind conditions. The area of the Swan Island group is 3 km^2 with an elongation in the direction of the prevailing wind. The land-fetch is 5 km at the balloon release point on the western end of the west island. The highest elevation is 25 m.

Monthly profiles at Swan Island point out an interesting seasonal variation of thermal wind. Diagram (a) of Fig. 9 shows three randomly chosen April hodographs and diagram (b), three July hodographs. These were obtained by averaging u and v components from all observations in each month. Note the monthly similarity from year to year and the marked difference between individual months. The April profiles closely resemble the normal trade-wind case of decreasing easterlies with height. However, in July the easterlies increase with height. This indicates an annual reversal of meridional temperature gradient (warm to the north in summer) in the vicinity of Swan Island, which is verified by the climatological sea-surface temperature averages presented by Riehl (1956).[3]

Statistics of individual observations also show the thermal wind effect on observed veering. At Ship N the average monthly horizontal sea and air temperature gradients were obtained from climatic atlases.

---

[3]The horizontal temperature gradient in the thermal wind equation is that of the air, not of the surface. However, over the tropical oceans, the temperature in the well mixed sub-cloud layer closely follows the sea-surface temperature.

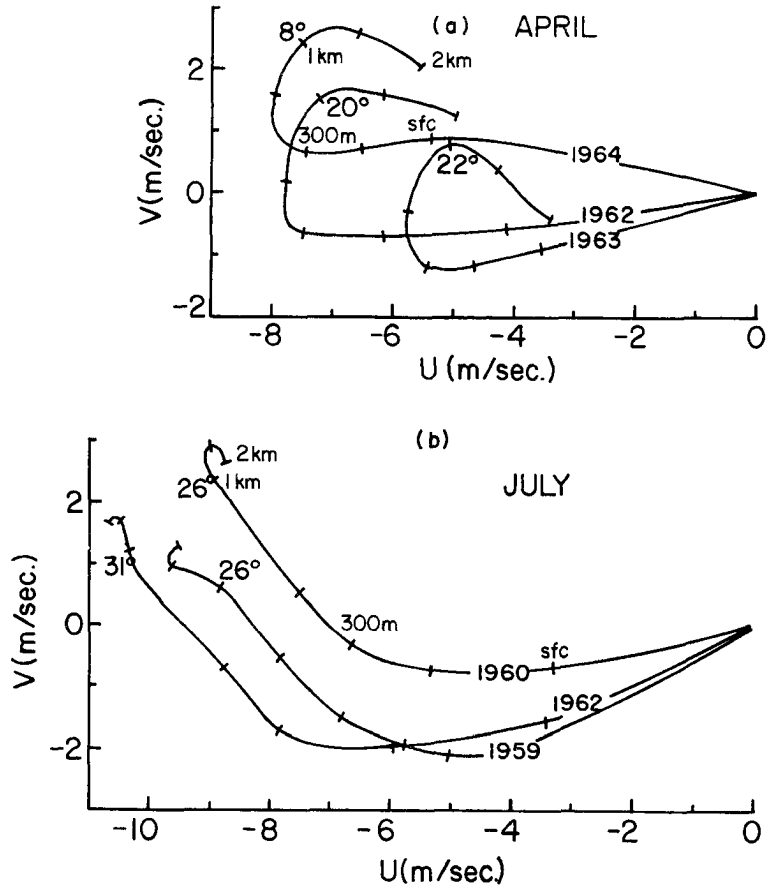

Fig. 9. Typical (a) April and (b) July hodographs at Swan Island showing effect of reversal of meridional temperature gradient within the veering layer. Elevation marks are shown at the surface, 150, 300, 500, 1000, 1500, and 2000 m. Average veering between the surface and 1000 m is shown for each month.

These gradients were assumed to exist through the lowest 1 km layer. Geostrophic veering was computed for each observation through the thermal wind equation. Observed veering was then averaged by 5° classes of geostrophic veering. Fig. 10 shows the average observed veering as a function of geostrophic veering at Ship N. The vertical distance between the lines indicates frictional veering. This amounts to approximately 10°.

Veering was also compared with surface wind direction at Ship N. Fig. 11 portrays the median veering in the surface to 500 m layer by overlapping 90° class intervals of surface direction. The much larger veering with southerly winds is shown. Observed veering from the surface to 1000 m indicates an even greater difference between northerly and southerly winds.

Plots similar to Fig. 10 of observed vs. geostrophic veering are shown in Figs. 12, 13, and 14 for Johnston Island, Ships I and J (after Findlater et al., 1966), and Shreveport, respectively. The corrected frictional veering at Johnston is approximately 10°. The veering data of Ships I and J were summarized by Findlater (op. cit.) in 8 classes of 900 mb wind direction. For purposes of the geostrophic veering computation the median wind speed at 900 mb was assumed the same for all wind direction classes. A constant thermal wind throughout the year was also used since the monthly averages of sea-surface temperature gradients do not differ appreciably from the yearly mean. With these assumptions the median frictional veering at I and J is found to be about 7°.

It must be emphasized that all the above computations have been made without regard to thermal stability which has a negligible diurnal variation over the oceans. However, Shreveport experiences a strong diurnal variation of lapse rate. For this reason Shreveport data were

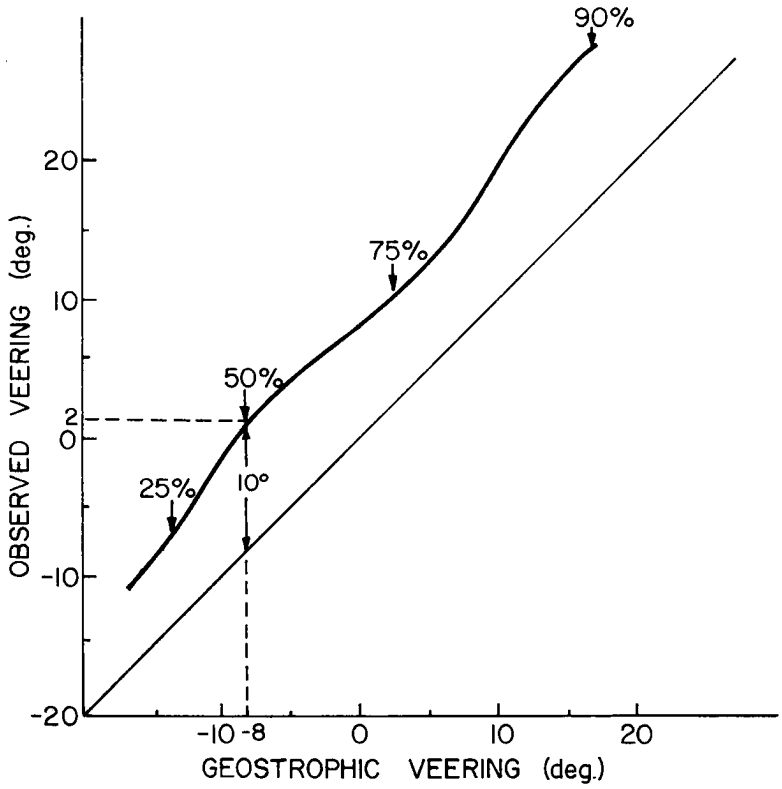

Fig. 10. Observed veering in the surface to 900 mb layer at Ship N as a function of geostrophic veering, obtained by averaging observed veering in 5° class intervals of geostrophic veering. The heavy line connects these average values. The dashed lines indicate that the median ("50%") geostrophic veering is - 8° and that the median observed veering is 2°. The difference of 10° is the median frictional veering. The thin sloping line connects points of equal observed and geostrophic veering, or where frictional veering equals zero. The vertical distance between the lines thus represents frictional veering and is indicated by arrows at the median point. The "75%" mark indicates that 75% of the observations had geostrophic veering of less than 3°, etc. Sample size: 2386 observations.

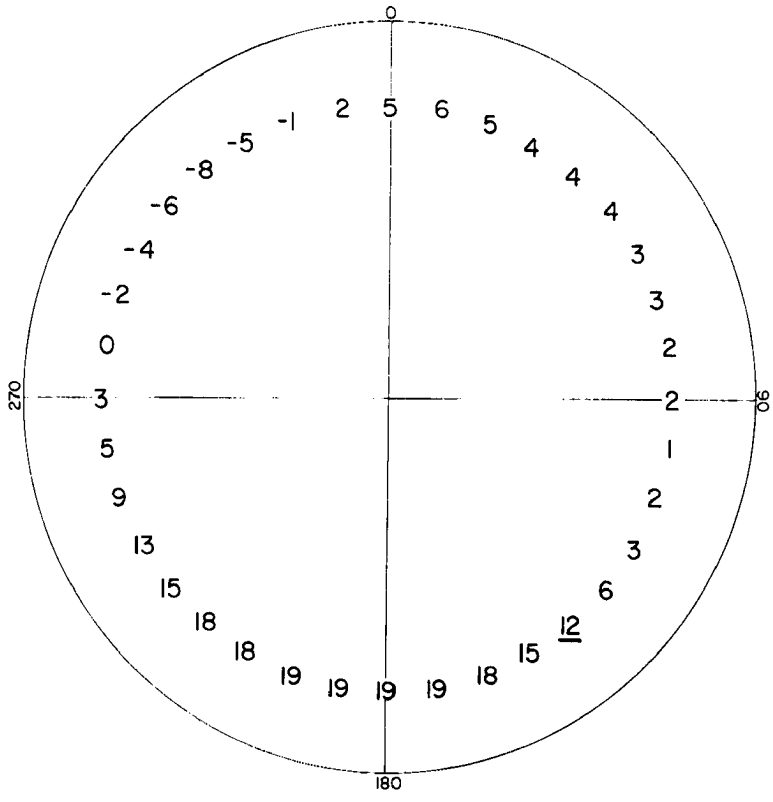

Fig. 11. Median observed veering in the surface to 500 mb layer at Ship N separated by overlapping 90° surface wind direction groups. (For example, median veering for cases of surface wind from 095° through 185° was 12°, indicated by the underlined number.)

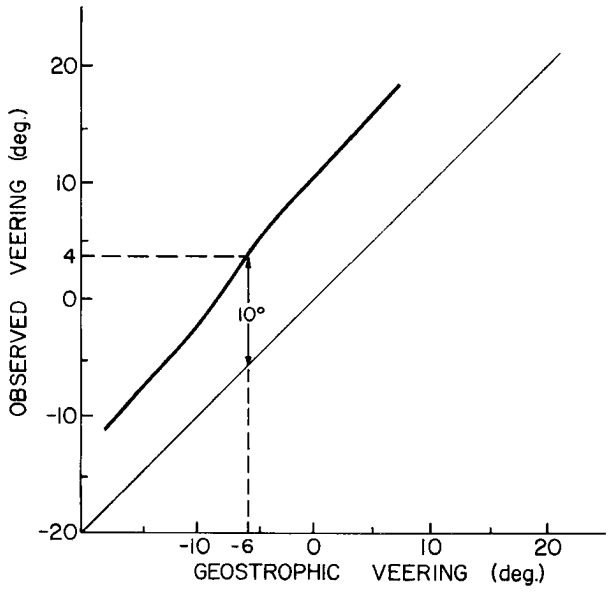

Fig. 12. Observed veering in the surface to 900 mb layer at Johnston Island as a function of geostrophic veering. (See Fig. 10 for further description.) Dashed lines indicate median geostrophic veering of - 6° and median observed veering of 4°. Difference of 10° is median frictional veering. Sample size: 3667 observations.

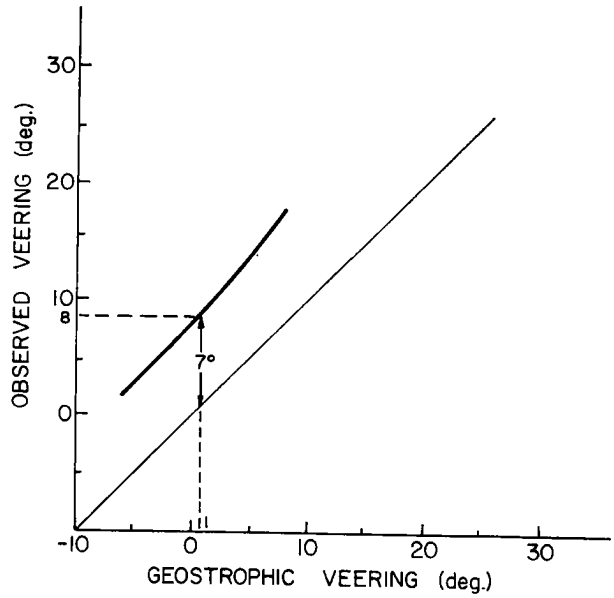

Fig. 13. Observed veering in the surface to 900 mb layer at Ships I and J as a function of geostrophic veering. (See Fig. 10 for further description.) The median frictional veering of 7° is indicated by arrows. (Original data after Findlater et al., 1966.)

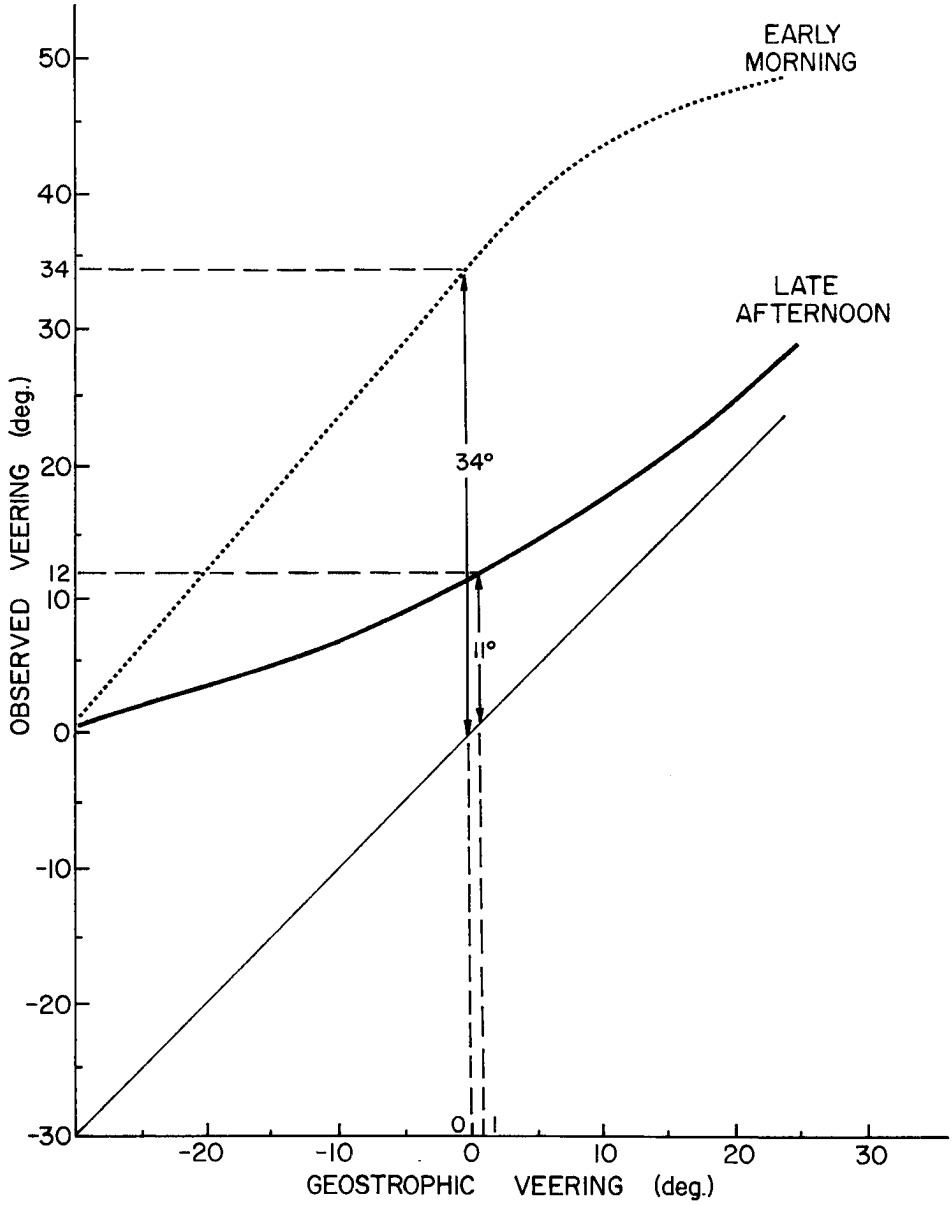

Fig. 14. Observed veering in the surface to 900 mb layer as a function of geostrophic veering at Shreveport for early morning and late afternoon observations separately. (See Fig. 10 for further description.) Median frictional veering is 34° in morning and 11° in afternoon. Sample size: 901 (morning); 956 (afternoon).

separated into morning (0500 local time) and afternoon (1700 local time) groups. Fig. 14 shows that the frictional veering at Shreveport is, in general, considerably greater in the early morning hours than in the late afternoon. Discussion of this important difference is left to the next section.

THE INFLUENCE OF THERMAL STABILITY ON OBSERVED VEERING

Vertical momentum transport in the planetary boundary layer affects the mechanical coupling between the surface and higher levels. Changes of thermal stability can act to increase or inhibit these momentum transports and thus affect the frictional veering.

Lapse rate is used as a stability parameter in this paper since no better variable related to vertical exchange is routinely measured. The applicability of lapse rate is suggested by comparison of wind veering and lapse rate frequency distributions. Fig. 15 demonstrates the large difference between morning and afternoon observed veering at Shreveport. The modal values indicated on the diagram show this difference to be about 37° for the surface to 950 mb layer. Fig. 16 gives the lapse rate distributions for the same layer and observation times. These figures clearly suggest, but of course do not prove, a strong correlation between observed veering and lapse rate.

In order to compare the observations at various stations, geostrophic veering must first be eliminated before frictional veering can be related to lapse rate. The failure to eliminate the rotation of the pressure gradient with height has been a source of error in previous studies. Fig. 17 shows the relationship between veering and lapse rate when geostrophic veering has been removed. The ordinate of this diagram may now be correctly labeled "frictional veering."

The Shreveport data of Fig. 17 show that frictional veering increases over land, as expected. Also of interest is the greater veering in the morning compared to afternoon for the same lapse value. It is likely that over land the lapse rate is quantitatively underestimated during

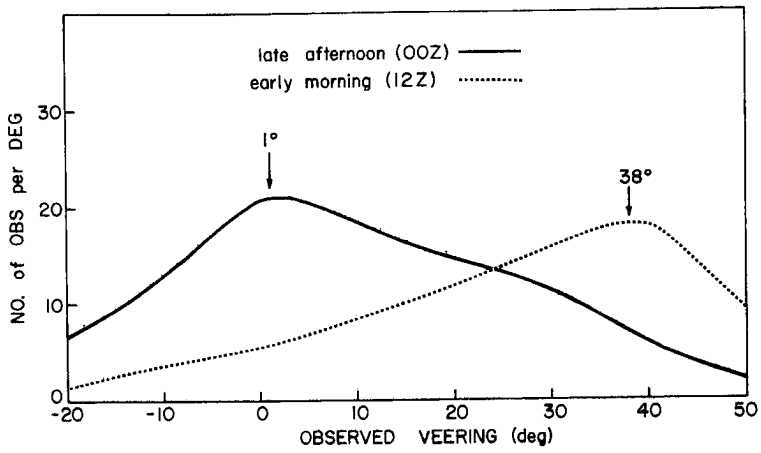

Fig. 15. Smoothed frequency distributions of veering in surface to 950 mb layer at Shreveport by time of day. Balloon release times are 0500 local (morning) and 1700 local (afternoon). Arrows indicate veering at peak of each distribution. Sample size: 901 (morning); 956 (afternoon).

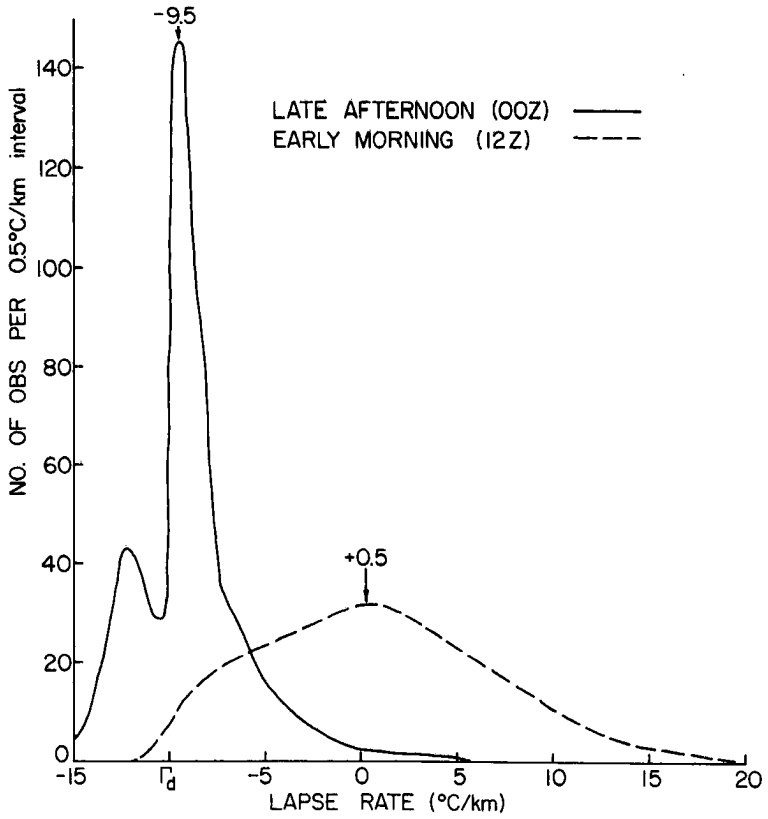

Fig. 16. Smoothed frequency distributions of lapse rate in surface to 950 mb layer at Shreveport by time of day. Balloon release times are 0500 local (morning) and 1700 local (afternoon). Arrows indicate lapse rate at peak of each distribution. Γ_d is the dry adiabatic lapse rate.

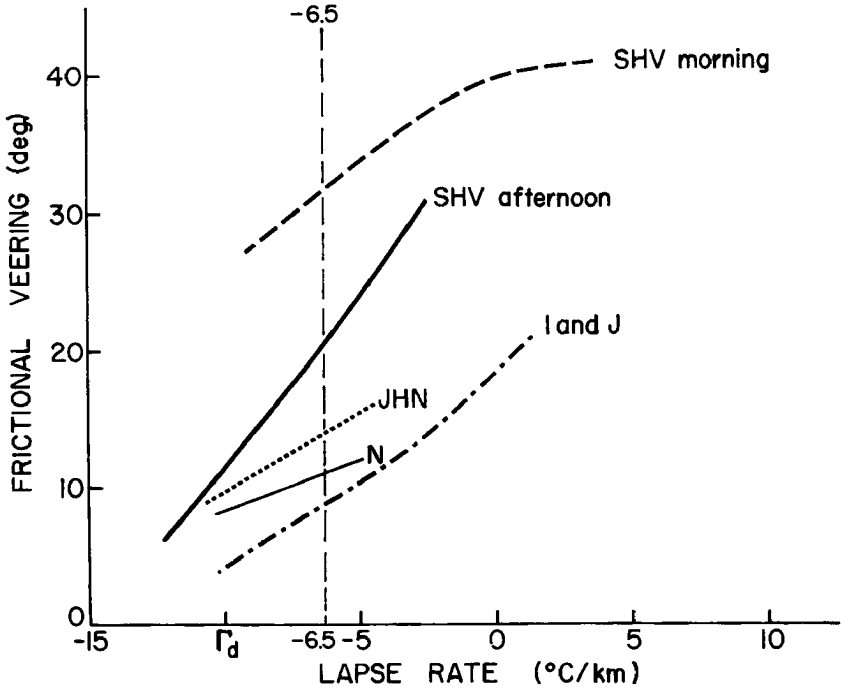

Fig. 17. Frictional veering (with geostrophic veering effect accounted for and removed) as a function of lapse rate in the surface to 900 mb layer at each station. Smooth lines were obtained by averaging frictional veering in classes of lapse rate and connecting the points.

nighttime since the top of the inversion is often below the 900 mb level. Thus, the layer may have a measured isothermal lapse rate but actually contain a low-level inversion. A better scheme would more accurately account for the strength and height of the inversion. An inversion inhibits vertical mixing; thus, a single parameter characterizing the strength of this barrier would be useful. Such a classification could not be attempted in this study without data at significant levels (i.e., the exact levels of the bottom and top of the inversion or other levels where the lapse rate changes significantly).

Wind and temperature data from the WKY-TV tower in Oklahoma City (instrumented by the National Severe Storms Laboratory) were also investigated.[4] Fig. 18 compares hourly values of wind veering between the 146 and 1459 ft levels and lapse rate between the surface and 1459 ft level. The portrayed four-day period was chosen because the horizontal temperature gradient in the area was approximately zero and wind speed remained above 3 m/sec. With few exceptions, a strong correlation between lapse rate and veering is found. The cross-correlation coefficient reaches a maximum with wind veering lagging lapse rate by 1 hr. This lag indicates that changes of veering follow changes of lapse rate.

The backing of the wind with height during afternoon superadiabatic conditions can be explained in theory by an increase with height of the shearing stress (Sheppard et al., 1952). This implies a large increase with height of the vertical eddy exchange coefficient which is probably related to increased size and velocity of the gust-scale eddies in unstable condition.

---

[4] Continuous recordings are made on this tower at seven levels between the surface and 1459 ft using Aerovane wind instruments and thermistor temperature sensors.

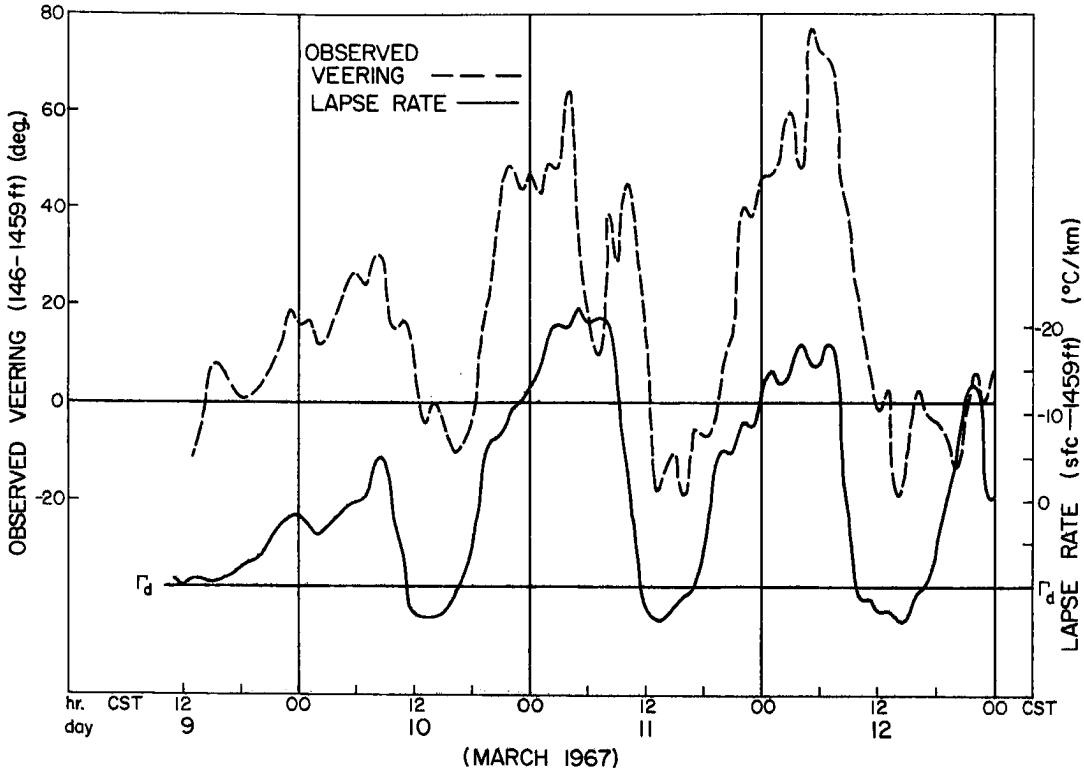

Fig. 18. Time-series of wind veering and lapse rate at the WKY-TV tower, Oklahoma City, for the period 9-12 March 1967. Values were taken every 5 min from the analogue records and then averaged over 1 hr intervals.

Intuitively, one would expect an increase in depth of the friction layer with decreasing stability. Such a relation can also be derived from Ekman theory. This raises the possibility that our choice of 900 mb as the level of "no friction" is too high at night and too low in the daytime. Thus, total daytime veering may be slightly larger than measured. Fig. 19 does, however, show that most of the wind veering at Shreveport occurs below 950 mb. In a large statistical study of wind veering over the tropical oceans, Gray (1967) has observed mean veering to be small above 900 mb.

The next section describes the combined influences on observed veering of thermal stability and geostrophic veering.

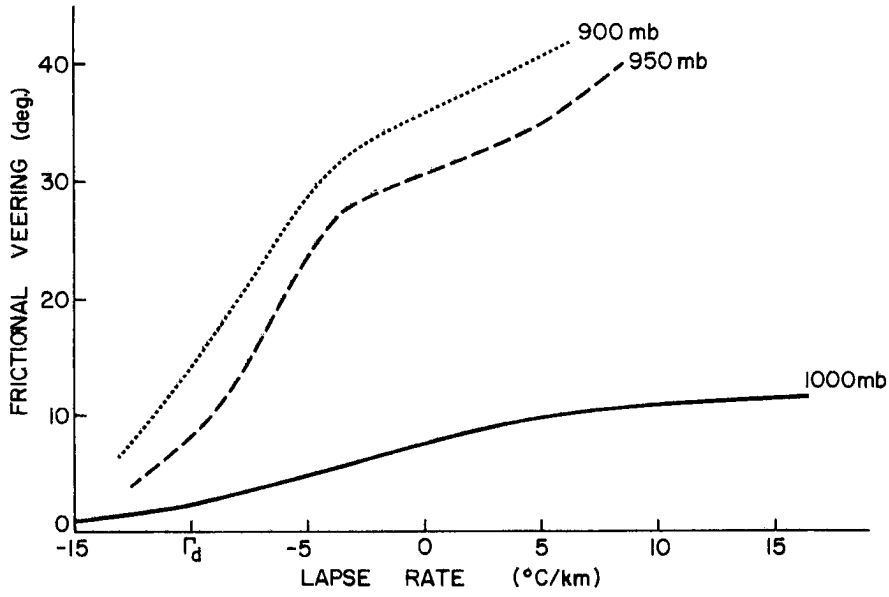

Fig. 19. Frictional veering (with geostrophic veering effect accounted for and removed) as a function of lapse rate at Shreveport for the layers from surface to indicated pressure level. Morning and afternoon data are combined. Note that most of the frictional veering occurs between the surface and 950 mb. Sample size: 1857 observations.

OBSERVED VEERING AS A FUNCTION OF BOTH LAPSE RATE AND GEOSTROPHIC VEERING

In addition to diabatic effects (e.g., radiational cooling or heating of the ground), lapse rate can be varied by differential advection. These effects are additive--advection of cold air over a warm surface tends to steepen the lapse rate[5] and both, in turn, tend to decrease observed veering. Thus, the role of either parameter may be overestimated if considered by itself.

For purposes of this analysis, two criteria--geostrophic veering and lapse rate--were used to define a veering class. For example, referring to the heavily outlined box of Fig. 21, there were 118 cases of lapse rate between -6 and -10°C/km in which the geostrophic veering was simultaneously between 0° and -10°, indicated by the upper number. Classes in which there were less than 10 observations are omitted as are all individual observations with absolute value of observed veering greater than 90° or with wind speed less than 3 m/sec. Wind speeds greater than 20 m/sec were rarely observed. In Figs. 21-23, isolines (dashed) of average observed veering at Shreveport have been drawn to the average values in the boxes. Figs. 24-26 portray conditions for the oceanic stations. Smaller class intervals are used for these stations since the parameter variations are less. For comparison they are, however, plotted on the scale used for Shreveport.

---

[5] Evidence of this interaction is given in Fig. 20 which shows the average lapse rate (sfc to 950 mb) at Ship N in classes of surface wind direction. Though the difference is not large, smaller lapse rates generally occur with southerly winds, which usually indicate warm advection at Ship N.

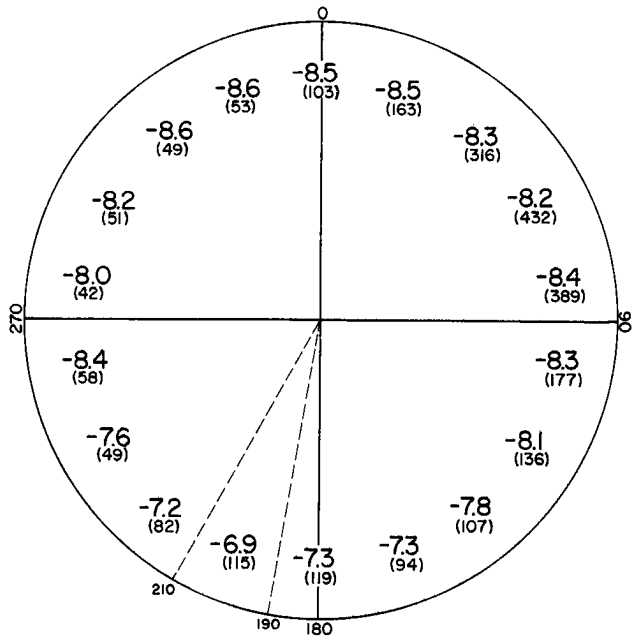

Fig. 20. Average lapse rate in the surface to 950 mb layer at Ship N by classes of surface wind direction. (For example, the average lapse rate for the 115 cases of surface wind from 190° through 210° was - 6.9°C/km.) The smaller lapse rates with southerly winds indicate that warm advection (positive geostrophic veering) tends to stabilize the lapse rate.

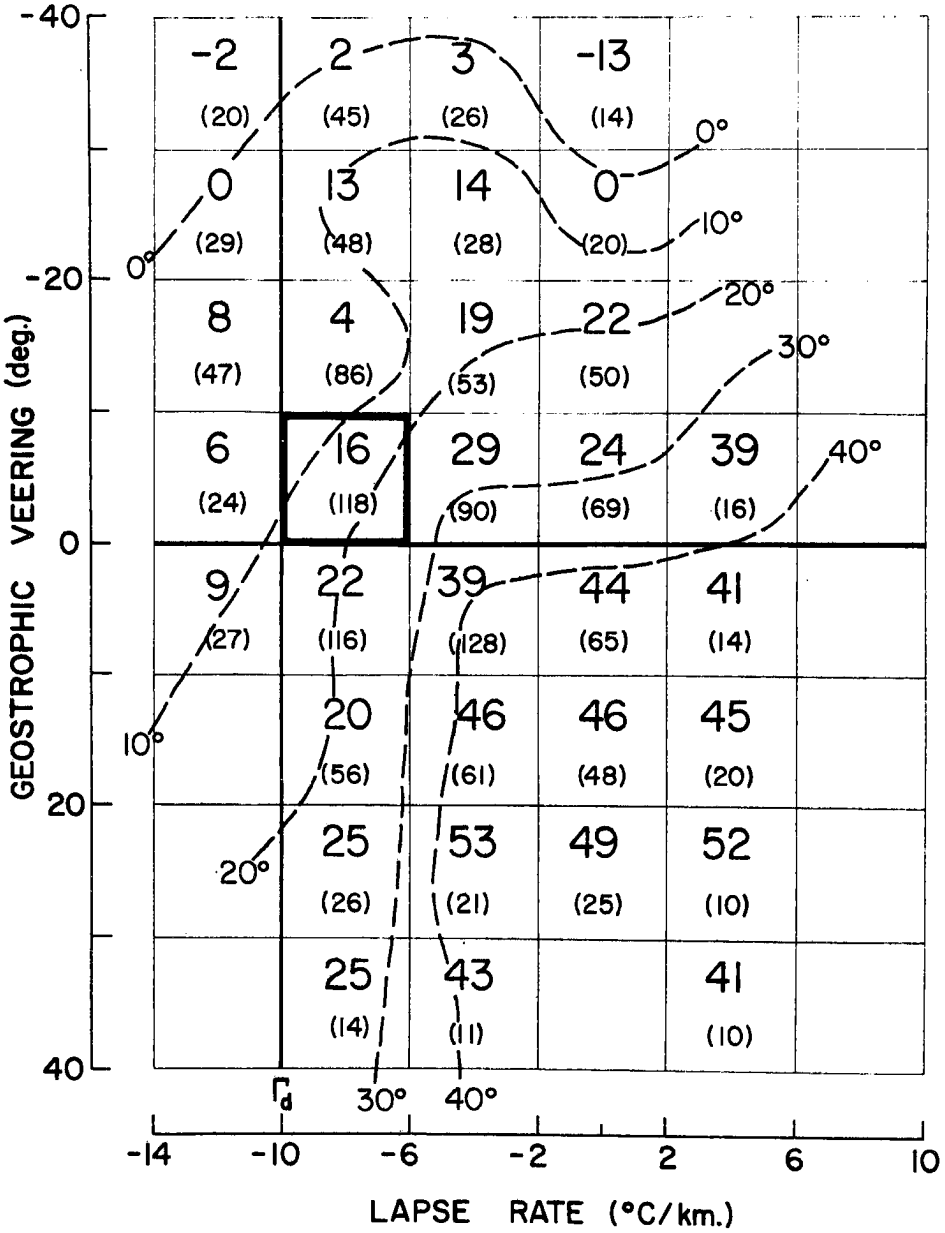

Fig. 21. Observed veering (surface - 900 mb) at Shreveport as a function of lapse rate and geostrophic veering. (For example, the heavily outlined box refers to the 118 cases of lapse rate between - 6° and - 10° C/km in which the geostrophic veering was simultaneously between 0° and - 10°. The average observed veering for this class was 16°, indicated by the upper number.) Approximate isolines of observed veering are drawn to the average values in the boxes.

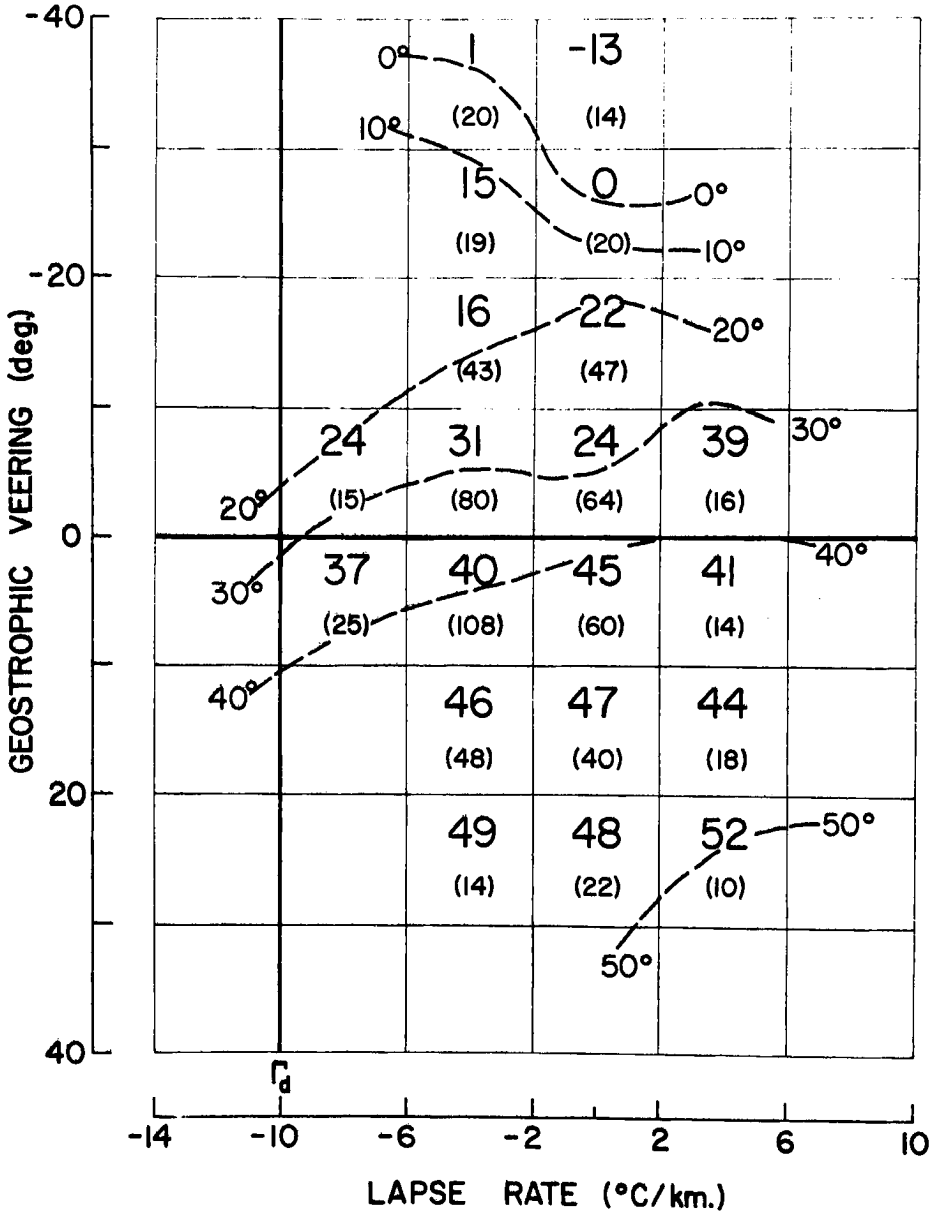

Fig. 22. Observed veering (surface - 900 mb) at Shreveport as a function of lapse rate and geostrophic veering for morning observations (1200GMT or 0500 local) only. See Fig. 21 for explanation.

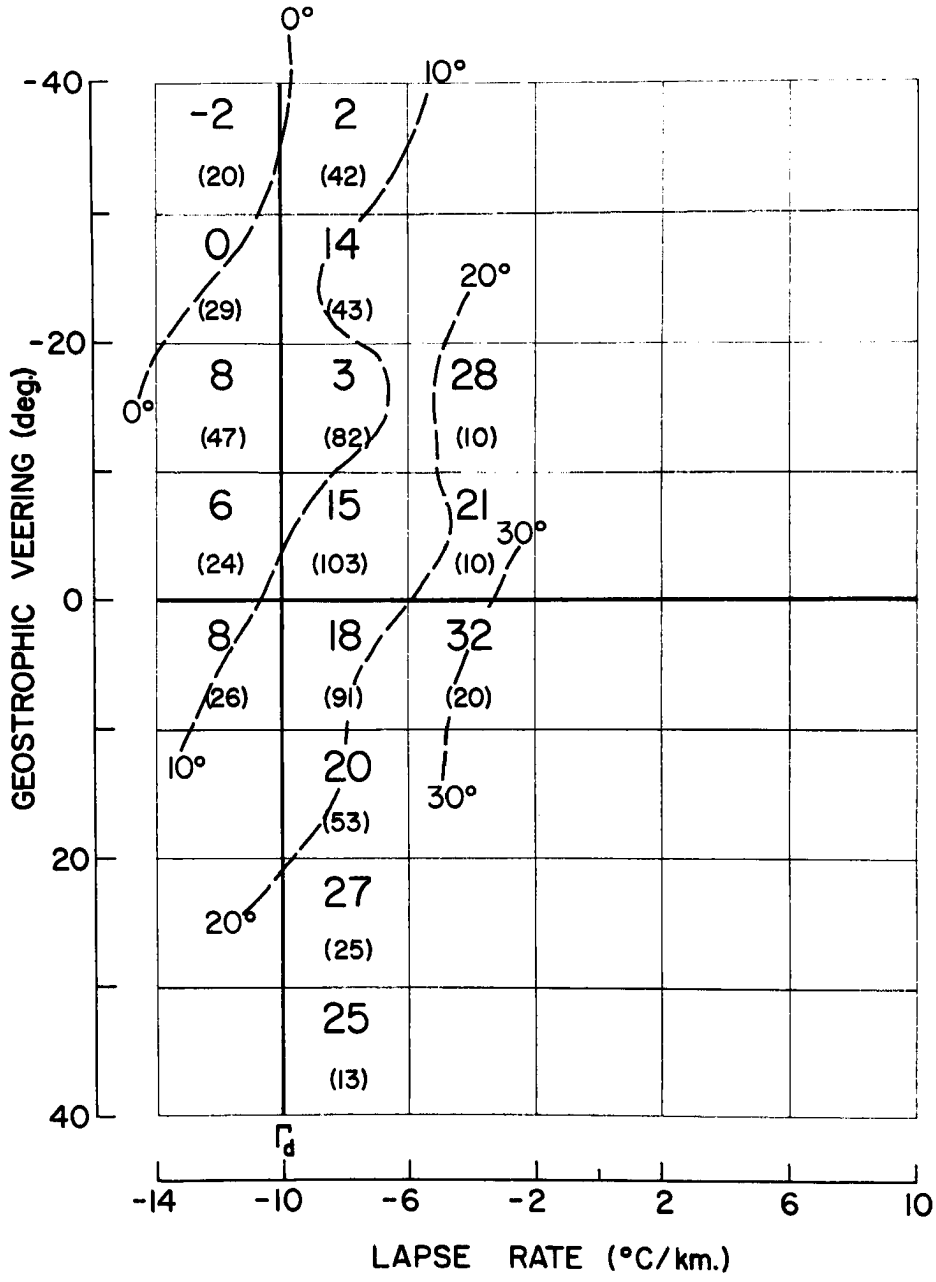

Fig. 23. Observed veering (surface - 900 mb) at Shreveport as a function of lapse rate and geostrophic veering for afternoon observations (0000GMT or 1700 local) only. See Fig. 21 for explanation.

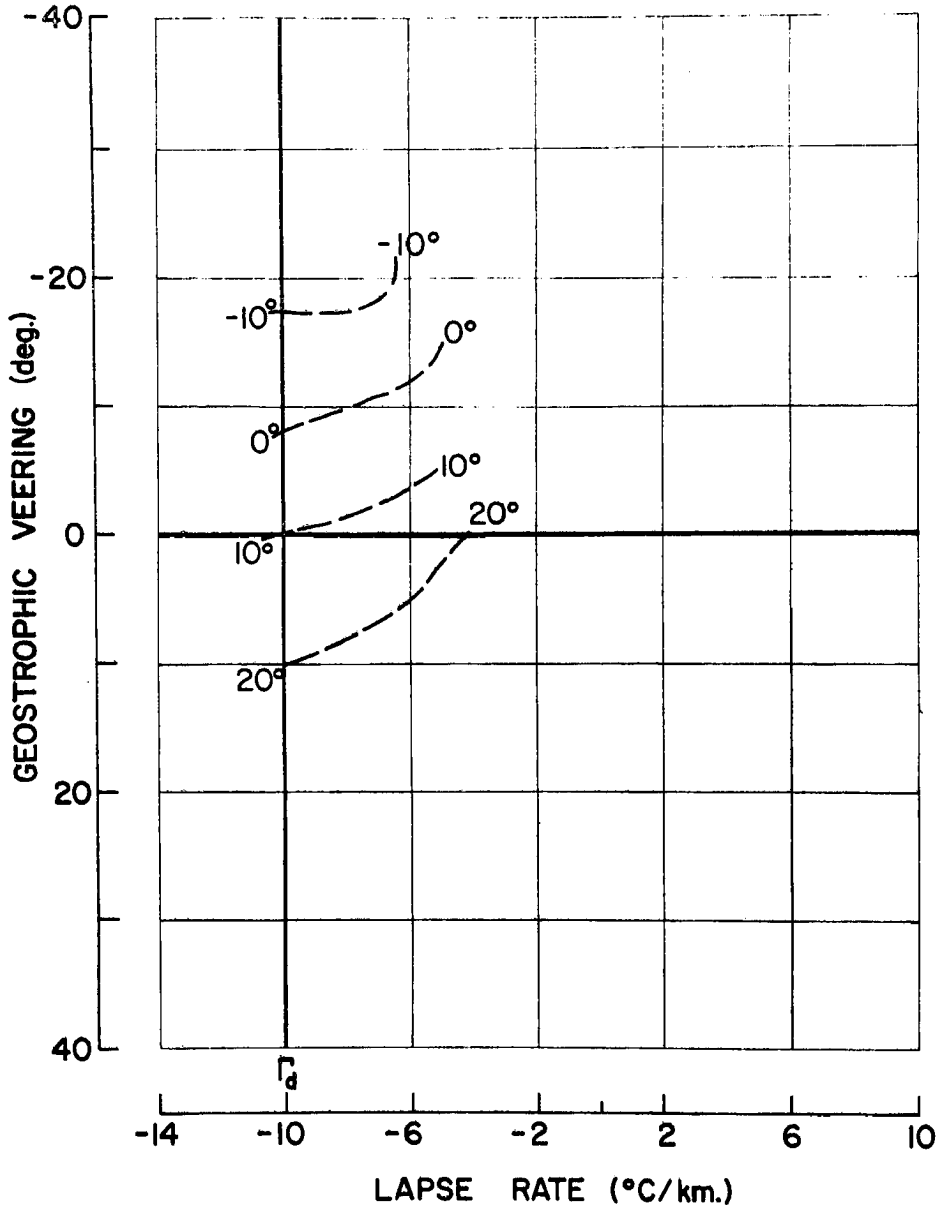

Fig. 24. Isolines of average observed veering (surface-900 mb) at Ship N as a function of lapse rate and geostrophic veering. Sample size: 2386 observations. See Fig. 21 for explanation.

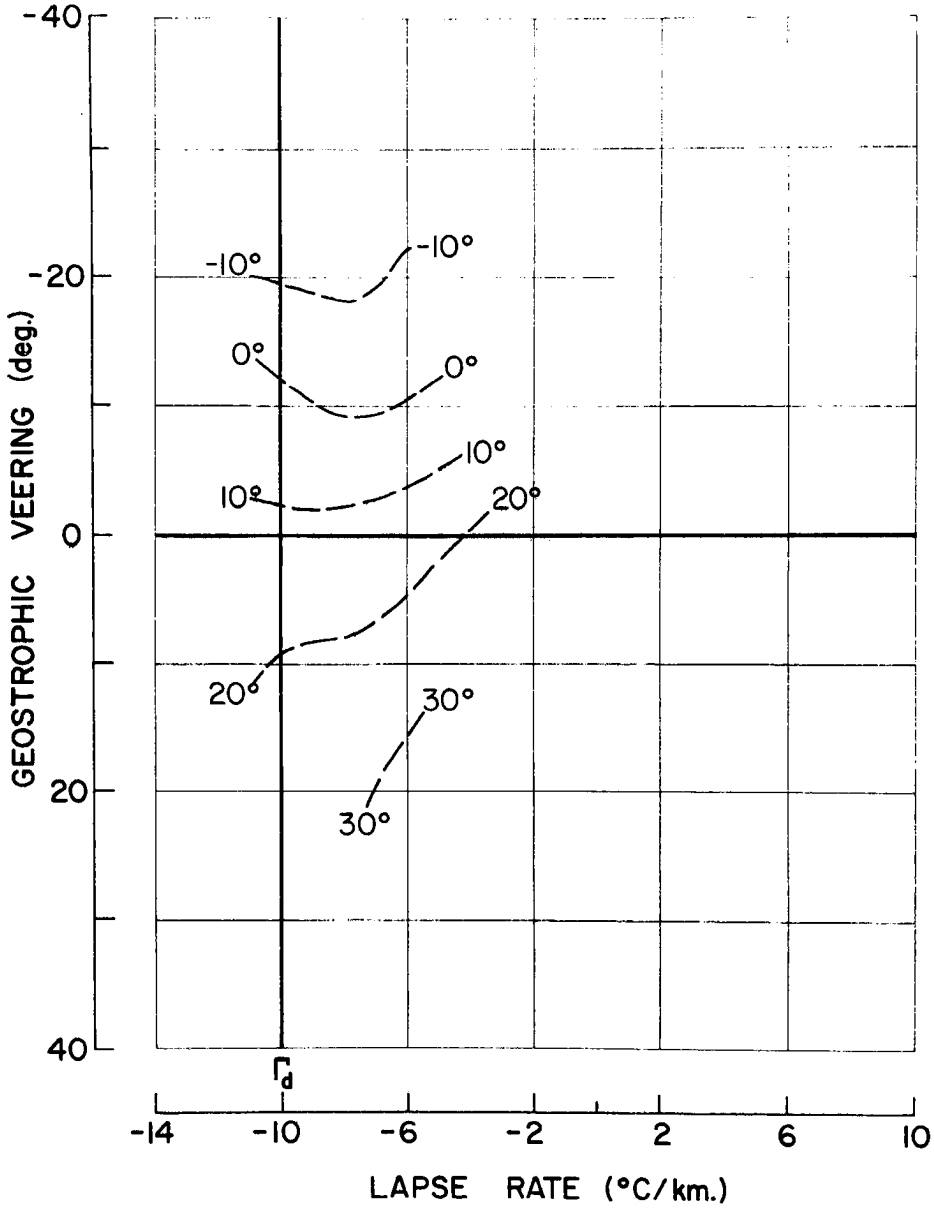

Fig. 25. Isolines of average observed veering (surface-900 mb) at Johnston Island as a function of lapse rate and geostrophic veering. Sample size: 3696 observations. See Fig. 21 for explanation.

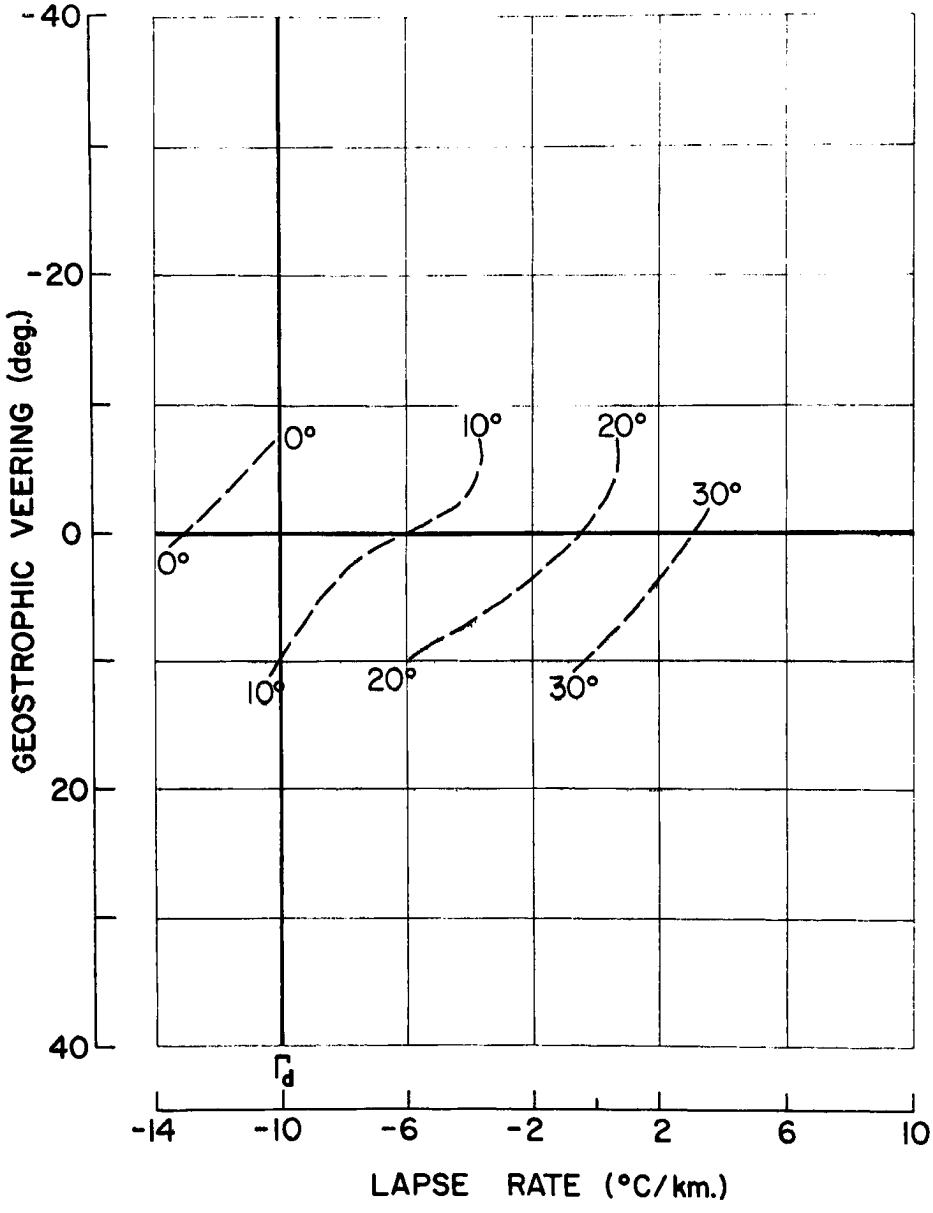

Fig. 26. Isolines of average observed veering (surface-900 mb) at Ships I and J as a function of lapse rate and geostrophic veering. (Original data from Findlater et al., 1966.) See Fig. 21 for explanation.

The relative importance of lapse rate compared to geostrophic veering can be seen by the slopes of the observed veering isolines. Geostrophic veering becomes more important as the lines tend towards the horizontal. Thus, changes of observed veering at Ship N and Johnston result almost entirely from changes in the geostrophic veering. Table 2 summarizes the approximate slopes of the observed veering isolines for each station in terms of inclination angle from the horizontal.

TABLE 2

Approximate slopes of the observed veering isolines in Figs. 22-26, showing the relative importance of geostrophic veering and lapse rate.

Station	Isoline slope (deg.)	
Johnston Island	10	(geostr. veering important)
Ship N	15	"
Ships I and J	40	(both important)
Shreveport - morning	15	(lapse class. inaccurate)
Shreveport - afternoon	70	(lapse rate most important)

The variation in relative importance of lapse rate and geostrophic veering from place to place is attributed, in large part, to the variability of the parameters themselves. It seems reasonable that lapse rate and geostrophic veering should have an implicit relationship to observed veering. Thus, veering at Johnston is physically related to lapse rate but the lapse rate is almost constant and therefore does not appear as a variable factor. Fig. 27 compares the surface to 900 mb lapse rate distributions at all the stations. Note that the more peaked distributions correspond to the stations in Table 2 with smaller isoline

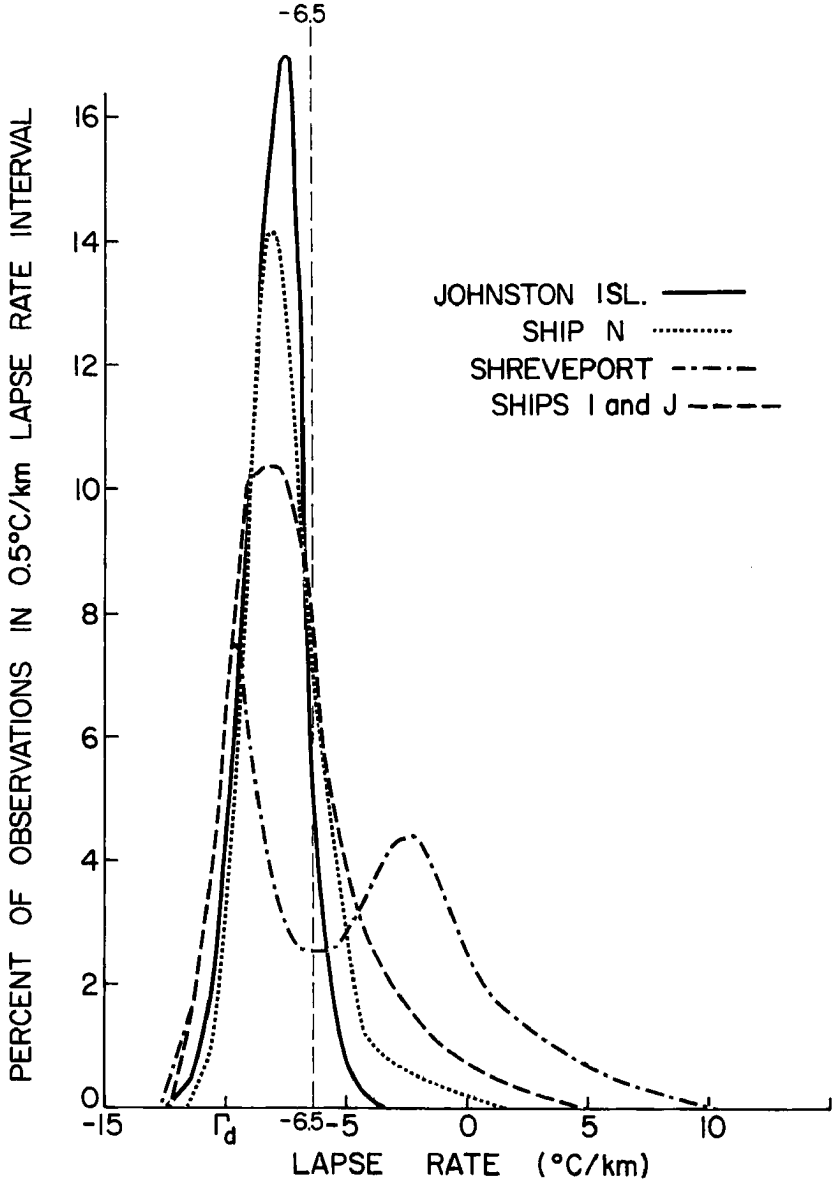

Fig. 27. Normalized frequency distributions of lapse rate in surface to 900 mb layer.

slopes. The exception is Shreveport - morning, where the lapse rate classification is inaccurate in inversion situations.

Classification of Wind Veering Regimes

In order to compare veering at the different stations on an equivalent basis, a lapse rate correction was made in addition to the one for geostrophic veering. The correction for thermal stability was taken as the difference between the average frictional veering at a station and the frictional veering for a lapse rate of - 6.5°C/km (U.S. Standard Atmosphere), obtained from Fig. 17. For example, the mean frictional veering in the afternoon at Shreveport is 11° but increases to 19° at the standard lapse rate. (See Fig. 17.) The lapse rate correction is thus + 8°. Table 3 gives the average observed veering, individual corrections for geostrophic veering and lapse rate, and the final corrected veering at each station. These final values can now be compared to show the effects of differing surface roughness. Actual frictional veering is observed to be smaller over the oceans. The large veering at Swan Island indicates its rough topography. Frictional veering was not found to increase with increasing wind speed at any of the stations.

Fig. 28 shows the data of Table 3 in graphical form. The case of southerly surface winds at Ship N is also included. The lapse rate correction at Shreveport is largest (either positive or negative) while the geostrophic veering correction is most important at the ocean stations.

The corrected veering values of Table 3 lead to surface stress and drag coefficient calculations that are somewhat more realistic

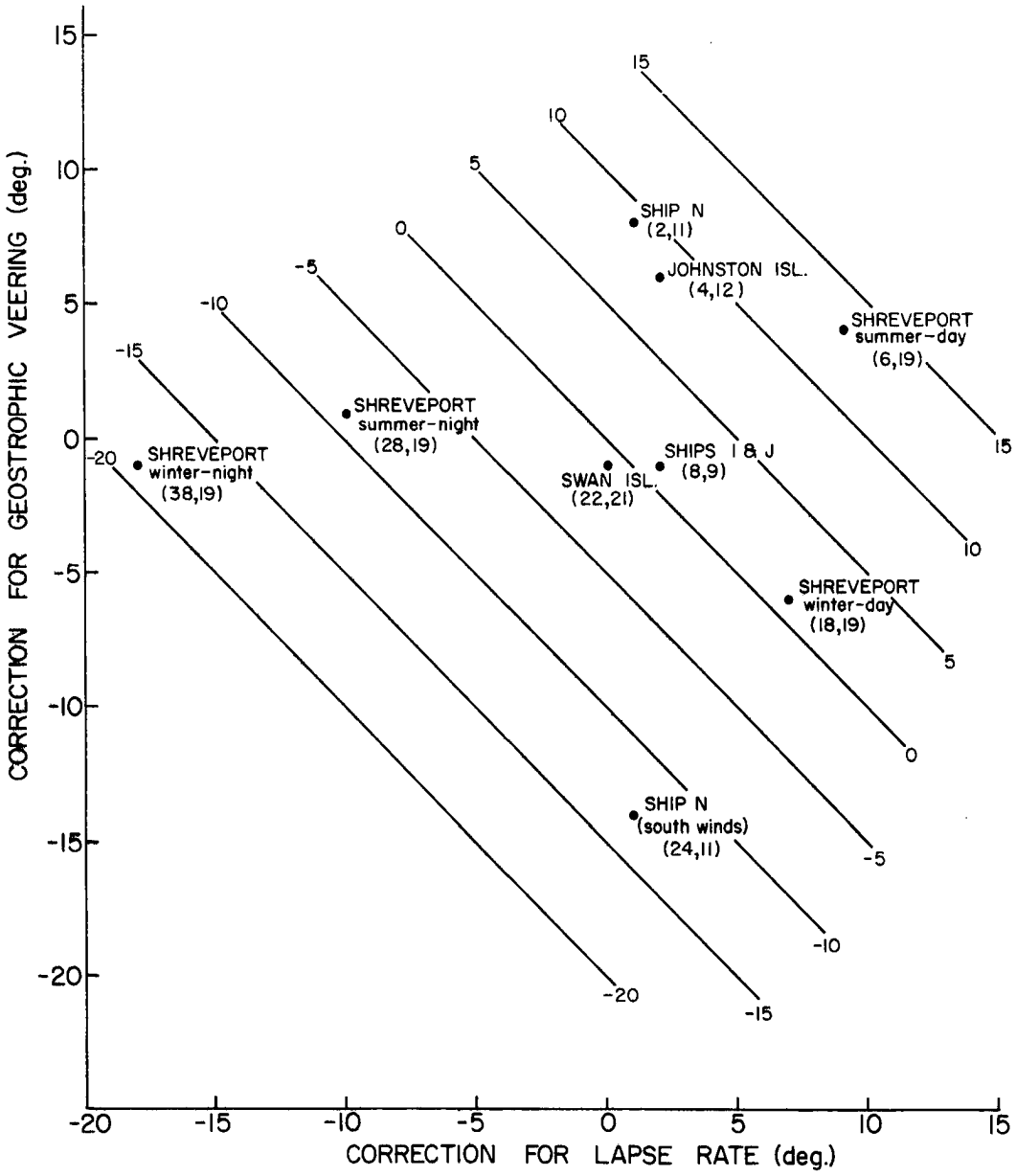

Fig. 28. Correction graph to obtain frictional veering in layer from surface to 900 mb for stations with mean lapse rate and mean geostrophic veering different from assumed standard conditions of zero geostrophic veering and - 6. 5°C/km lapse rate. Numbers in parentheses indicate average observed veering and corrected veering, respectively. Sloping lines give the total correction (sum of lapse rate and geostrophic corrections).

TABLE 3

Correction table to obtain frictional veering for standard conditions of zero geostrophic veering and - 6.5°C/km lapse rate in the surface to 900 mb layer. All values in degrees.

station	median observed veering	correction			corrected veering
		geostr. veering	lapse rate	total	
Shreveport					
summer day	6	+4	+9	+13	19
summer night	28	+1	-10	-9	19
winter day	18	-6	+7	+1	19
winter night	38	-1	-18	-19	19
Johnston Island	4	+6	+2	+8	12
Ship N	2	+8	+1	+9	11
Ships I and J	8	-1	+2	+1	9
Swan Island	22	-1	0	-1	21

than those obtained from observed data. The median observed veering of 2° at Ship N corresponds to a drag coefficient (C_D) of only 0.2×10^{-3} if no thermal wind or pressure gradient rotation correction is applied (i.e., if the geostrophic wind is assumed to be constant with height and equal to the observed wind at 1 km). After correction by the geostrophic departure method (see, e.g., Sheppard and Omar, 1952), C_D is computed to be 1.3×10^{-3}. The average C_D from 51 separate studies summarized by Roll (1965) is 1.8×10^{-3}. The typical value at Shreveport is 1.9×10^{-3}.

Fig. 29 shows a classification of wind veering regimes by the type of variability of the lapse rate and geostrophic veering corrections. Four types of variability are recognized, viz., diurnal, synoptic, diurnal and synoptic, and steady or seasonal. Regimes not covered

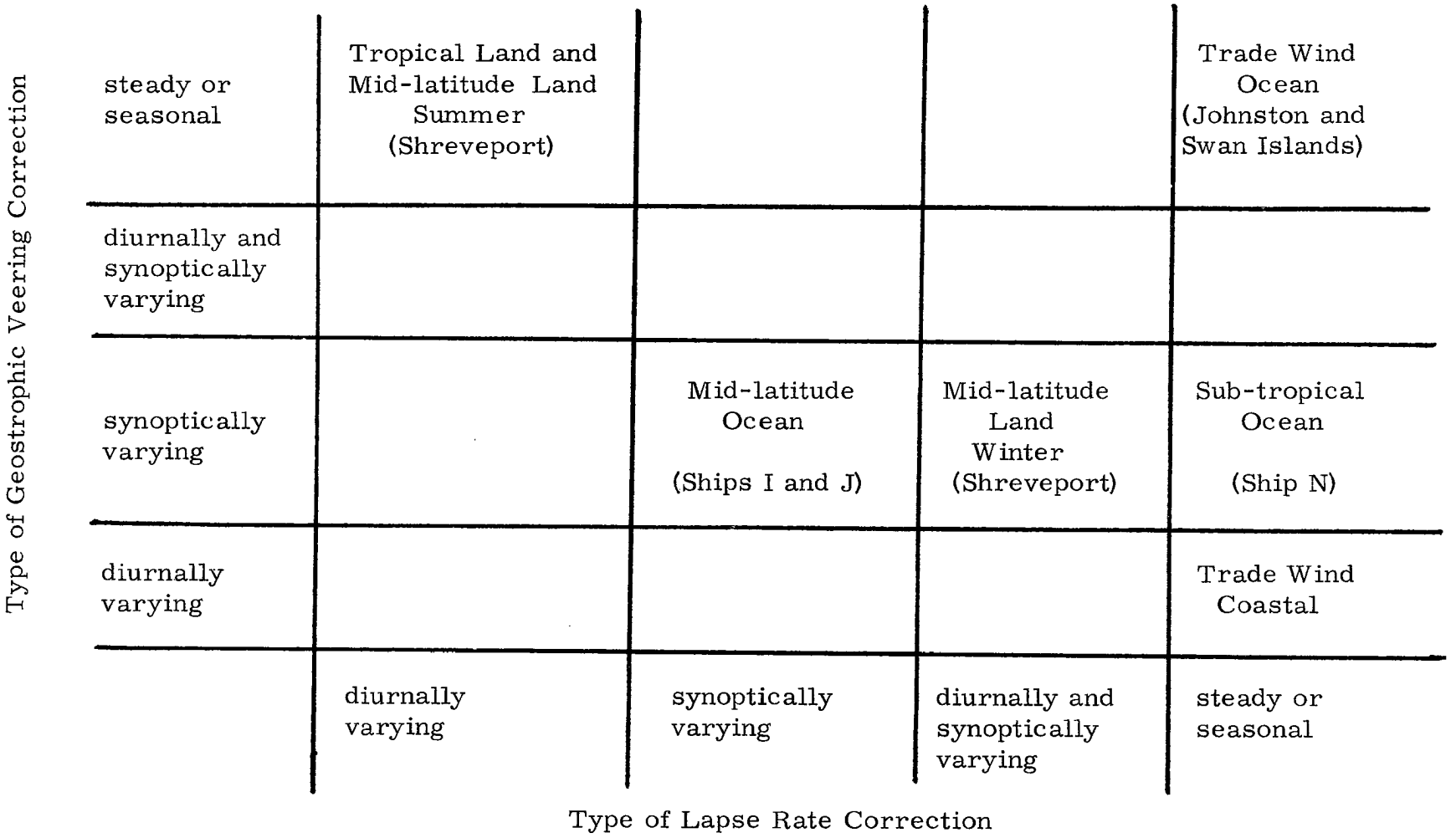

Fig. 29. Type of geostrophic veering and lapse rate corrections needed to obtain frictional veering in various climatic regimes.

in this paper are shown in parentheses and those with contradictory conditions are left blank. The main regime included without supporting data is "trade-wind land" where thermal advection is generally small and constant but lapse rate varies diurnally. The Shreveport - summer observations are similar to this regime. Also recognized is the special case of "trade-wind coastal" where thermal advection changes are caused by diurnal land-sea temperature differences, but lapse rate variations are small.

The regimes studied in this paper are listed below with representative stations and general characteristics:

1) Trade Wind Ocean (Johnston and Swan Islands). Lapse rate variation is very small. Geostrophic veering is almost constant. It is consistently negative at Johnston Island, weakly positive at Swan Island.

2) Sub-tropical Ocean (Ship N). Middle-latitude synoptic influences are occasionally felt. Lapse rate is relatively constant. Slightly steeper lapse rates are noted in cold advection, however. Surface wind direction is more variable than in the trade winds. This causes substantial variations in geostrophic veering. As in 1) above, variations in geostrophic veering are most important.

3) Mid-latitude Ocean (Ships I and J). As in all oceanic regions, diurnal variability is small. A continuous progression of synoptic disturbances causes associated variations in lapse rate and geostrophic veering. In this regime both geostrophic veering and lapse rate are important in explaining veering.

4) Mid-latitude Land - Summer (Shreveport). Lapse rate has a strong diurnal variation. Synoptic disturbances do not penetrate region. Tropical characteristics are present. Lapse rate has the greater influence on observed veering.

5) Mid-latitude Land - Winter (Shreveport). Both diurnal and synoptic variations are important. Strong thermal advection is observed in frontal passages. In this regime both horizontal and vertical temperature gradients must be considered. The effect of lapse rate is especially important.

SUMMARY DISCUSSION

Conclusions

Wind veering in the planetary boundary layer is highly variable from one observation to the next, even in the relatively steady trades. Part of this variability is due to random, small-scale eddies and can be eliminated by taking long-period averages. However, average profiles at the individual stations still deviate appreciably from a simple Ekman spiral. An approach to a more reasonable profile is obtained at each station after making corrections for horizontal and vertical temperature gradients.

In general, observed veering is decreased in cold advection (negative geostrophic or pressure gradient veering) and in thermal instability (steep lapse rates). In the northeast trades, for example, observed veering is very small due to continuous cold advection. A larger veering is obtained after applying the geostrophic veering correction. This leads to more reasonable surface stress and drag coefficient values. The lapse rate correction becomes most important over land because of the large diurnal variability of stability which causes observed veering to increase greatly in nighttime inversions.

After adjustment for pressure gradient rotation and lapse rate, an actual frictional veering over the oceans of about 10° is obtained. Corrected veering over land is approximately 20°.

No correlation between veering and wind speed was found.

Recommendations

The mechanically induced turbulence in the planetary boundary layer is of such magnitude that only a statistical approach has a

reasonable chance of delineating the general veering characteristics of the wind. There is a limit to which the theoretical developments can be extended without firm observational backing. With modern computer techniques and with the availability of large amounts of accessible data at Asheville, the necessary material is at our disposal. In future studies it would seem that further advances to our understanding of the boundary layer could come from an empirical approach.

ACKNOWLEDGMENTS

The author wishes to express his sincere appreciation to Professor William M. Gray, who proposed and directed this research and gave countless hours of guidance and counsel.

Thanks are also due the National Weather Records Center, ESSA, Asheville, North Carolina, for supplying the radiosonde data; to the National Severe Storms Laboratory, ESSA, Norman, Oklahoma, for the tower data; and to the National Center for Atmospheric Research, Boulder, Colorado, for their grant of computer time.

This project was sponsored by the National Science Foundation and the Environmental Science Services Administration.

Hess, S. L., 1959: Introduction to Theoretical Meteorology. Henry Holt and Co., New York, 362 pp. (Ch. 18, "Viscosity and Turbulence.")

Jehn, K. H., and S. J. Durie, 1963: Boundary-layer wind maxima and associated temperature distributions as observed on the 1400-foot television tower near Dallas, Texas 1961-1962. Scientific Report No. 1, Electrical Engineering Research Laboratory, University of Texas.

Johnson, W. B. Jr., 1962: Climatology of atmospheric boundary-layer parameters and energy dissipation. Studies of the Three-Dimensional Structure of the Planetary Boundary Layer, Department of Meteorology, University of Wisconsin, 125-158.

_____, 1965: Atmospheric boundary-layer dynamics over the forests of northeastern Wisconsin. Studies of the Effects of Variations in Boundary Conditions on the Atmospheric Boundary Layer, Department of Meteorology, University of Wisconsin, 45-145.

Lettau, B., 1967: Thermally and frictionally produced wind shear in the planetary boundary layer at Little America, Antarctica. Monthly Weather Review, 95, 627-634.

Lettau, H. H., and H. Hoeber, 1964: Über die Bestimmung der Höhenverteilung von Schubspannung und Austauschkoeffizient in der atmosphärischen Reibungsschicht. Beiträge zur Physik der freien Atmosphäre, 37, 105-118.

Mildner, P., 1933: Über die Turbulenz des Windes, beobachtet mit Hilfe von doppelt und einfach visierten Pilotballonen. Beiträge zur Physik der freien Atmosphäre, 20, 144-176.

Nansen, F., 1902: Oceanography of the North Polar basin. The Norwegian North Polar Expedition 1893-96, Scientific Results, 3(9).

NAVAIR (U. S. Naval Air Systems Command), 1966: Selected Level Temperatures and Dew Points for the Northern Hemisphere, NAVAIR 50-1C-52).

Author: Bruce R. Mendenhall

551.554
551.551.25

A STATISTICAL STUDY OF FRICTIONAL WIND VEERING IN THE PLANETARY BOUNDARY LAYER

Colorado State University, Department of Atmospheric Science

Subject Headings:
Wind Profiles
Frictional Wind Veering
Boundary Layer Wind
Turbulence

National Science Foundation Grant No. GF-177
Environmental Science Services Administration Grant No. E-34-67(G)

An observational study of wind veering in the lowest 2 km at various global locations is presented. The turbulent variability of veering is eliminated in the statistical treatment by considering large data samples. Average wind profiles and statistics of the individual observations are computed in order to determine which large-scale parameters significantly affect observed veering. Corrections to observed veering are made for the horizontal temperature gradient (rotation of pressure gradient with height) and for variations of thermal stability. The relative importance of these corrections and the nature of their variability in different climatic regions are discussed. After statistically eliminating the unsteady effects and applying corrections for horizontal and vertical temperature gradients, a more characteristic spiral is obtained at each station.

Author: Bruce R. Mendenhall

551.554
551.551.25

A STATISTICAL STUDY OF FRICTIONAL WIND VEERING IN THE PLANETARY BOUNDARY LAYER

Colorado State University, Department of Atmospheric Science

Subject Headings:
Wind Profiles
Frictional Wind Veering
Boundary Layer Wind
Turbulence

National Science Foundation Grant No. GF-177
Environmental Science Services Administration Grant No. E-34-67(G)

An observational study of wind veering in the lowest 2 km at various global locations is presented. The turbulent variability of veering is eliminated in the statistical treatment by considering large data samples. Average wind profiles and statistics of the individual observations are computed in order to determine which large-scale parameters significantly affect observed veering. Corrections to observed veering are made for the horizontal temperature gradient (rotation of pressure gradient with height) and for variations of thermal stability. The relative importance of these corrections and the nature of their variability in different climatic regions are discussed. After statistically eliminating the unsteady effects and applying corrections for horizontal and vertical temperature gradients, a more characteristic spiral is obtained at each station.

Author: Bruce R. Mendenhall

551.554
551.551.25

A STATISTICAL STUDY OF FRICTIONAL WIND VEERING IN THE PLANETARY BOUNDARY LAYER

Colorado State University, Department of Atmospheric Science

Subject Headings:
Wind Profiles
Frictional Wind Veering
Boundary Layer Wind
Turbulence

National Science Foundation Grant No GF-177
Environmental Science Services Administration Grant No. E-34-67(G)

An observational study of wind veering in the lowest 2 km at various global locations is presented. The turbulent variability of veering is eliminated in the statistical treatment by considering large data samples. Average wind profiles and statistics of the individual observations are computed in order to determine which large-scale parameters significantly affect observed veering. Corrections to observed veering are made for the horizontal temperature gradient (rotation of pressure gradient with height) and for variations of thermal stability. The relative importance of these corrections and the nature of their variability in different climatic regions are discussed. After statistically eliminating the unsteady effects and applying corrections for horizontal and vertical temperature gradients, a more characteristic spiral is obtained at each station.